



OXFORD CENTRE FOR COLLABORATIVE APPLIED MATHEMATICS

Report Number 11/63

**Front propagation in stochastic neural fields**

by

**Paul C. Bressloff and Matthew A. Webber**



Oxford Centre for Collaborative Applied Mathematics  
Mathematical Institute  
24 - 29 St Giles'  
Oxford  
OX1 3LB  
England



# FRONT PROPAGATION IN STOCHASTIC NEURAL FIELDS\*

PAUL C. BRESSLOFF<sup>†</sup> AND MATTHEW A. WEBBER<sup>‡</sup>

**Abstract.** We analyse the effects of extrinsic multiplicative noise on front propagation in a scalar neural field with excitatory connections. Using a separation of time scales, we represent the fluctuating front in terms of a diffusive-like displacement (wandering) of the front from its uniformly translating position at long time scales, and fluctuations in the front profile around its instantaneous position at short time scales. One major result of our analysis is a comparison between freely propagating fronts and fronts locked to an externally moving stimulus. We show that the latter are much more robust to noise, since the stochastic wandering of the mean front profile is described by an Ornstein–Uhlenbeck process rather than a Wiener process, so that the variance in front position saturates in the long time limit rather than increasing linearly with time. Finally, we consider a stochastic neural field that supports a pulled front in the deterministic limit, and show that the wandering of such a front is now subdiffusive.

**Key words.** neural field, traveling fronts, multiplicative noise, stimulus-locking

**AMS subject classifications.** 92C20,

**1. Introduction.** Front propagation is a topic of ongoing interest in the study of nonequilibrium systems. Within the biological context, fronts describe a wide variety of processes including the spread of epidemics, the invasion of species, and biological evolution [35]. One fundamental result in the theory of deterministic fronts is the difference between fronts propagating into a linearly unstable state and those propagating into a metastable state (a state that is linearly stable but non-linearly unstable). In the latter case, the front has a unique velocity that is obtained by solving the associated PDE in traveling wave coordinates. The former, on the other hand, supports a continuum of possible velocities and associated traveling wave solutions; the particular velocity selected depends on the initial conditions. Fronts propagating into unstable states can be further partitioned into two broad categories: the so-called *pulled* and *pushed* fronts [46] emerging from sufficiently localized initial conditions. Pulled fronts propagate into an unstable state such that the asymptotic velocity is given by the linear spreading speed  $v^*$ , which is determined by linearizing about the unstable state within the leading edge of the front. That is, perturbations around the unstable state within the leading edge of the front grow and spread with speed  $v^*$ , thus “pulling along” the rest of the front. On the other hand, pushed fronts propagate into an unstable state with a speed greater than  $v^*$ , and it is the nonlinear growth within the region behind the leading edge that pushes the front speeds to higher values.

The properties of a deterministic front also play an important role in the effects of fluctuations (see the review by Panja [37]). In particular, pulled fronts are extremely sensitive to noise in the leading edge. Fluctuations arise when the underlying physical or biological substrate consists of discrete constituents interacting on a lattice (intrinsic noise), or when there are external environmental perturbations (extrinsic noise). In contrast to deterministic fronts, which asymptotically propagate with a fixed shape

---

\*This publication was based on work supported in part by the National Science Foundation (DMS-1120327) and by the Systems Biology Doctoral Training Centre, University of Oxford. We are also grateful for access to the Oxford Supercomputing Center.

<sup>†</sup>Department of Mathematics, University of Utah, Salt Lake City, UT 84112 USA (bressloff@math.utah.edu)

<sup>‡</sup>Mathematical Institute, University of Oxford, 24-29 St. Giles’, Oxford OX1 3LB, UK (matthew.webber@queens.ox.ac.uk)

and speed, different snapshots of one particular realization of a fluctuating front will have a different shape, and the position of the front at a fixed value (level set) will be a stochastic variable. Nevertheless, by performing an ensemble average over many realizations, it is often possible to represent the fluctuating front in terms of a mean front profile whose center of mass moves according to a Langevin equation with a constant drift velocity  $v$  and diffusivity  $D$  [34, 45, 38, 2, 44]. However, this relatively simple picture breaks down in the case of pulled fronts where, for example, the center of mass exhibits subdiffusive behavior [43].

In this paper, we extend the theory of fluctuating fronts to the case of stochastic neural fields. Neural fields represent the large-scale dynamics of spatially structured networks of neurons in terms of nonlinear integrodifferential equations, whose associated kernels represent the spatial distribution of neuronal synaptic connections. Such models provide an important example of spatially extended dynamical systems with nonlocal interactions. As in the case of nonlinear PDE models of reaction diffusion systems, neural fields can exhibit a rich repertoire of wave phenomena, including solitary traveling fronts, pulses and spiral waves [21, 16, 11]. They have been used to model wave propagation in cortical slices [39, 42] and *in vivo* [29]. A common *in vitro* experimental method for studying wave propagation is to remove a slice of brain tissue and bathe it in a pharmacological medium that blocks the effects of inhibition. Synchronized discharges can then be evoked by a weak electrical stimulus to a local site on the slice and each discharge propagates away from the stimulus at a characteristic speed of about 60 – 90 mm/s [40, 42]. These waves typically take the form of traveling pulses with the decay of activity at the trailing edge resulting from some form of local adaptation or refractory process. On the other hand, a number of phenomena in visual perception involve the propagation of a traveling front, in which a suppressed visual percept replaces a dominant percept within the visual field of an observer. A classical example is the wave-like propagation of perceptual dominance during binocular rivalry [47, 33, 31, 10]. Binocular rivalry is the phenomenon whereby perception switches back and forth between different images presented to the two eyes. The resulting fluctuations in perceptual dominance and suppression provide a basis for non-invasive studies of the human visual system and the identification of possible neural mechanisms underlying conscious visual awareness [5].

In the case of a scalar neural field equation with purely excitatory connections and a sigmoidal firing rate function, it can be proven that there exists a traveling front solution with a unique speed that depends on the firing threshold and the range/strength of synaptic weights [1, 20]. The wave thus has characteristics typical of a front propagating into a metastable state. Various generalizations of deterministic front solutions have also been developed in order to take into account the effects of network inhomogeneities [7, 17], external stimuli [25, 22], and network competition in a model of binocular rivalry waves [10]. As far as we are aware, however, there has been very little work on the effects of fluctuations on front propagation in neural fields. One notable exception is a study by Brackley and Turner [6], who consider a specific model of a neural field with a fluctuating threshold. Waves in stochastic neural fields are also briefly considered by Coombes *et. al.* [18], although their main emphasis is the effects of quenched noise. Here we develop a general theory of fluctuating fronts in neural fields with extrinsic multiplicative noise by adapting methods developed previously for PDEs [34, 45, 38, 2, 44]. Such methods exploit a separation of time scales in which there is a diffusive-like displacement (wandering) of the front from its uniformly translating position at long time scales, and fluctuations in the front profile

around its instantaneous position at short time scales. In the case of multiplicative noise under the Stratonovich interpretation, there is also a renormalization of the mean front velocity. In §2 and §3, we consider fronts propagating into a metastable state by taking the nonlinear firing rate function to be a sigmoid or Heaviside function. One major result of our analysis is a comparison between freely propagating fronts (see §2) and fronts locked to an externally moving stimulus (see §3). We show that the latter are much more robust to noise, since the center of mass of the front wanders according to an Ornstein–Uhlenbeck process rather than a Wiener process, so that the variance in front position saturates in the long time limit rather than increasing linearly with time. In §4, we consider a neural field equation that supports fronts propagating into an unstable state, which take the form of pulled rather than pushed fronts. We then show that multiplicative noise leads to a subdiffusive wandering of the front, as previously found for a reaction diffusion system [43].

Finally, note that there does not yet exist a rigorous multi-scale analysis of neural systems, in which continuum neural fields are derived from microscopic models of synaptically coupled spiking neurons. Such models would need to take proper account of noise-induced fluctuations and statistical correlations between neurons at multiple spatial and temporal scales. Consequently, current formulations of stochastic neural field theory tend to be phenomenologically based. One approach is to consider a Langevin version of the deterministic neural field equations involving some form of extrinsic spatiotemporal white noise [30, 23], which is the approach taken here. An alternative approach is to treat the deterministic neural field equations as the thermodynamic limit of an underlying master equation [13, 14, 8, 9]. In the latter case, a diffusion approximation leads to an effective Langevin equation with multiplicative noise.

## 2. Effects of multiplicative noise on freely propagating fronts.

**2.1. Deterministic scalar neural field.** Let us begin by briefly reviewing front propagation in a scalar neural field equation of the form

$$\tau \frac{\partial u(x, t)}{\partial t} = -u(x, t) + \int_{-\infty}^{\infty} w(x - x') F(u(x', t)) dx'. \quad (2.1)$$

Here  $u(x, t)$  is a measure of activity within a local population of excitatory neurons at  $x \in \mathbb{R}$  and time  $t$ ,  $\tau$  is a membrane time constant (of order 10 msec),  $w(x)$  denotes the spatial distribution of synaptic connections between local populations, and  $F(u)$  is a nonlinear firing rate function.  $F$  is often taken to be a sigmoid function

$$F(u) = \frac{1}{1 + e^{-\gamma(u-\kappa)}} \quad (2.2)$$

with gain  $\gamma$  and threshold  $\kappa$ . In the high-gain limit  $\gamma \rightarrow \infty$ , this reduces to the Heaviside function

$$F(u) \rightarrow H(u - \kappa) = \begin{cases} 1 & \text{if } u > \kappa \\ 0 & \text{if } u \leq \kappa \end{cases} \quad (2.3)$$

We will assume that the weight distribution is a positive, even function of  $x$ ,  $w(x) \geq 0$  and  $w(-x) = w(x)$ , and that  $w(x)$  is a monotonically decreasing function of  $x$  for  $x \geq 0$ . A common choice is the exponential weight distribution

$$w(x) = \frac{1}{2\sigma} e^{-|x|/\sigma}, \quad (2.4)$$

where  $\sigma$  determines the range of synaptic connections. The latter tends to range from  $100\mu\text{ m}$  to  $1\text{ mm}$ . We fix the units of time and space by setting  $\tau = 1, \sigma = 2$ .

A homogeneous fixed point solution  $U^*$  of equation (2.1) satisfies

$$U^* = W_0 F(U^*), \quad W_0 = \int_{-\infty}^{\infty} w(y) dy. \quad (2.5)$$

In the case of a sigmoid function with appropriately chosen gain and threshold, it is straightforward to show graphically that there exists a pair of stable fixed points  $U^*_{\pm}$  separated by an unstable fixed point  $U^*_0$ . In the high gain limit  $F(U) \rightarrow H(U - \kappa)$  with  $0 < \kappa < W_0$ , the unstable fixed point disappears and  $U^*_+ = W_0, U^*_- = 0$ . As originally shown by Amari [1], an explicit traveling front solution of equation (2.1) that links  $U^*_+$  and  $U^*_-$  can be constructed in the case of a Heaviside nonlinearity. In order to construct such a solution, we introduce the traveling wave coordinate  $\xi = x - ct$ , where  $c$  denotes the wavespeed, and set  $u(x, t) = \mathcal{U}(\xi)$  with  $\lim_{\xi \rightarrow -\infty} \mathcal{U}(\xi) = U^*_+ > 0$  and  $\lim_{\xi \rightarrow \infty} \mathcal{U}(\xi) = 0$  such that  $\mathcal{U}(\xi)$  only crosses the threshold  $\kappa$  once. Since equation (2.1) is equivariant with respect to uniform translations, we are free to take the threshold crossing point to be at the origin,  $\mathcal{U}(0) = \kappa$ , so that  $\mathcal{U}(\xi) < \kappa$  for  $\xi > 0$  and  $\mathcal{U}(\xi) > \kappa$  for  $\xi < 0$ . Substituting this traveling front solution into equation (2.1) with  $F(u) = H(u - \kappa)$  then gives

$$-c\mathcal{U}'(\xi) + \mathcal{U}(\xi) = \int_{-\infty}^0 w(\xi - \xi') d\xi' = \int_{\xi}^{\infty} w(x) dx \equiv W(\xi), \quad (2.6)$$

where  $\mathcal{U}'(\xi) = d\mathcal{U}/d\xi$ . Multiplying both sides of the above equation by  $e^{-\xi/c}$  and integrating with respect to  $\xi$  leads to the solution

$$\mathcal{U}(\xi) = e^{\xi/c} \left[ \kappa - \frac{1}{c} \int_0^{\xi} e^{-y/c} W(y) dy \right]. \quad (2.7)$$

Finally, requiring the solution to remain bounded as  $\xi \rightarrow \infty$  ( $\xi \rightarrow -\infty$ ) for  $c > 0$  (for  $c < 0$ ) implies that  $\kappa$  must satisfy the condition

$$\kappa = \frac{1}{|c|} \int_0^{\infty} e^{-y/|c|} W(\text{sign}(c)y) dy, \quad (2.8)$$

and thus

$$\mathcal{U}(\xi) = \frac{1}{c} \int_0^{\infty} e^{-y/c} W(y + \xi) dy. \quad (2.9)$$

Hence, one of the useful aspects of the constructive method is that it allows us to derive an explicit expression for the wavespeed as a function of physiological parameters such as the firing threshold. In the case of the exponential weight distribution (2.4), the relationship between wavespeed  $c$  and threshold  $\kappa$  is

$$c = c_+(\kappa) \equiv \frac{\sigma}{2\kappa} [1 - 2\kappa] \quad \text{for } \kappa < 0.5, \quad (2.10)$$

$$c = c_-(\kappa) \equiv \frac{\sigma}{2} \frac{1 - 2\kappa}{1 - \kappa} \quad \text{for } 0.5 < \kappa < 1.$$

This establishes the existence of a unique front solution for fixed  $\kappa$ , which travels to the right ( $c > 0$ ) when  $0 < \kappa < 0.5$  and travels to the left ( $c < 0$ ) when  $1 > \kappa > 0.5$ . Using Evans function techniques, it can also be shown that the traveling front is stable [48, 15]. Finally, given the existence of a traveling front solution for a Heaviside rate function, it is possible to prove the existence of a unique front in the case of a smooth sigmoid nonlinearity using a continuation method [20].

**2.2. Stochastic neural field with multiplicative noise.** Several recent studies have considered stochastic versions of neural field equations such as (2.1) that are based on a corresponding Langevin equation formulation [30, 23]. The extrinsic noise is typically taken to be additive, that is, independent of the activity state  $u$ . An alternative formulation of stochastic neural field theory has been developed in terms of a neural master equation [13, 14, 8, 9], in which the underlying deterministic equations are recovered in the thermodynamic limit  $N \rightarrow \infty$ , where  $N$  is a measure of the system size of each local population. In the case of large but finite  $N$ , a Kramers-Moyal expansion of the master equation yields a Langevin neural field equation with multiplicative noise [8, 9]. Motivated by these examples, we consider the following Langevin equation for the stochastic activity variable  $U(x, t)$ :

$$dU(x, t) = \left[ -U(x, t) + \int_{-\infty}^{\infty} w(x-y)F(U(y, t))dy \right] dt + \varepsilon^{1/2}g(U(x, t))dW(x, t) \quad (2.11)$$

We assume that  $dW(x, t)$  represents an independent Wiener process such that

$$\langle dW(x, t) \rangle = 0, \quad \langle dW(x, t)dW(x', t') \rangle = 2C([x-x']/\lambda)\delta(t-t')dt dt'. \quad (2.12)$$

Here  $\lambda$  is the spatial correlation length of the noise such that  $C(x/\lambda) \rightarrow \delta(x)$  in the limit  $\lambda \rightarrow 0$ , and  $\varepsilon$  determines the strength of the noise, which is assumed to be weak. The multiplicative factor  $g(U)$  could arise from some form of Langevin approximation of a neural master equation, or reflect some form of parametric noise such as threshold noise [6]. The multiplicative noise term is taken to be of Stratonovich form [27].

The effects of multiplicative noise on front propagation can be analyzed using methods previously developed for reaction-diffusion equations [34, 45, 38, 2, 44]; we will follow the particular formulation of Armero *et. al.* [2]. The starting point of such methods is the observation that multiplicative noise in the Stratonovich sense leads to a systematic shift in the mean speed of the front (assuming a front of speed  $c$  exists when  $\varepsilon = 0$ ). This is a consequence of the fact that  $\langle g(U)dW \rangle \neq 0$  even though  $\langle dW \rangle = 0$ . The former average can be calculated using Novikov's theorem [36]:

$$\varepsilon^{1/2}\langle g(U)dW \rangle = \varepsilon C(0)\langle g'(U)g(U) \rangle dt. \quad (2.13)$$

An alternative way to derive the above result is to Fourier transform equation (2.11) and evaluate averages using the corresponding Fokker-Planck equation in Fourier space (see appendix and [44]). Note that in the limit  $\lambda \rightarrow 0$ ,  $C(0) \rightarrow 1/\Delta x$  where  $\Delta x$  is a lattice cut-off, which can be identified with the step size of the spatial discretization scheme used in numerical simulations. Following [2], it is convenient to rewrite equation (2.11) so that the fluctuating term has zero mean:

$$dU(x, t) = \left[ h(U(x, t)) + \int_{-\infty}^{\infty} w(x-y)F(U(y, t))dy \right] dt + \varepsilon^{1/2}dR(U, x, t), \quad (2.14)$$

where

$$h(U) = -U + \varepsilon C(0)g'(U)g(U) \quad (2.15)$$

and

$$dR(U, x, t) = g(U)dW(x, t) - \varepsilon^{1/2}C(0)g'(U)g(U)dt. \quad (2.16)$$

The stochastic process  $R$  has zero mean (so does not contribute to the effective drift, that is, the average wave speed) and variance

$$\langle dR(U, x, t)dR(U, x', t) \rangle = \langle g(U(x, t))dW(x, t)g(U(x', t))dW(x', t) \rangle + \mathcal{O}(\varepsilon^{1/2}). \quad (2.17)$$

The next step in the analysis is to assume that the fluctuating term in equation (2.14) generates two distinct phenomena that occur on different time-scales: a diffusive-like displacement of the front from its uniformly translating position at long time scales, and fluctuations in the front profile around its instantaneous position at short time scales [34, 45, 38, 2, 44]. In particular, following [2], we express the solution  $U$  of equation (2.14) as a combination of a fixed wave profile  $U_0$  that is displaced by an amount  $\Delta(t)$  from its uniformly translating mean position  $\xi = x - c_\varepsilon t$ , and a time-dependent fluctuation  $\Phi$  in the front shape about the instantaneous position of the front:

$$U(x, t) = U_0(\xi - \Delta(t)) + \varepsilon^{1/2}\Phi(\xi - \Delta(t), t). \quad (2.18)$$

Here  $c_\varepsilon$  denotes the mean speed of the front. To a first approximation, the stochastic variable  $\Delta(t)$  undergoes Brownian motion with a diffusion coefficient  $D(\varepsilon) = \mathcal{O}(\varepsilon)$  (see below), which represents the effects of slow fluctuations, whereas  $\Phi$  represents the effects of fast fluctuations. Note that the expansion (2.18) is not equivalent to a standard small-noise expansion, since the wave profile  $U_0$  implicitly depends on  $\varepsilon$ . Indeed, substituting equation (2.18) into equation (2.14) and taking averages generates to leading order the following deterministic equation for  $U_0$ :

$$-c_\varepsilon \frac{dU_0}{d\xi} - h(U_0(\xi)) = \int_{-\infty}^{\infty} w(\xi - \xi')F(U_0(\xi'))d\xi'. \quad (2.19)$$

Both the mean speed  $c_\varepsilon$  and  $U_0$  depend non-trivially on the noise strength  $\varepsilon$  due to the  $\varepsilon$ -dependence of the function  $h$ , see equation (2.15). Thus,  $c_\varepsilon \neq c$  for  $\varepsilon > 0$  and  $c_0 = c$ , where  $c$  is the speed of the front in the absence of multiplicative noise. Proceeding to the next order and imposing equation (2.19), we find that  $\Delta(t) = \mathcal{O}(\varepsilon^{1/2})$  and

$$d\Phi(\xi, t) = \widehat{L} \circ \Phi(\xi, t)dt + \varepsilon^{-1/2}U_0'(\xi)d\Delta(t) + dR(U_0, \xi, t) \quad (2.20)$$

where  $\widehat{L}$  is the non-self-adjoint linear operator

$$\widehat{L} \circ A(\xi) = c_\varepsilon \frac{dA(\xi)}{d\xi} + h'(U_0(\xi))A(\xi) + \int_{-\infty}^{\infty} w(\xi - \xi')F'(U_0(\xi'))A(\xi')d\xi' \quad (2.21)$$

for any function  $A(\xi) \in L_2(\mathbb{R})$ .

It can be shown that for a sigmoid firing rate function and exponential weight distribution, the operator  $\widehat{L}$  has a 1D null space spanned by  $U_0'(\xi)$  [20]. (The fact that  $U_0'(\xi)$  belongs to the null space follows immediately from differentiating equation (2.19) with respect to  $\xi$ ). We then have the solvability condition for the existence of a nontrivial solution of equation (2.20), namely, that the inhomogeneous part is orthogonal to all elements of the null space of the adjoint operator  $\widehat{L}^*$ . The latter is defined with respect to the inner product

$$\int_{-\infty}^{\infty} B(\xi)\widehat{L}A(\xi)d\xi = \int_{-\infty}^{\infty} [\widehat{L}^*B(\xi)] A(\xi)d\xi \quad (2.22)$$

where  $A(\xi)$  and  $B(\xi)$  are arbitrary integrable functions. Hence,

$$\widehat{L}^* B(\xi) = -c_\varepsilon \frac{dB(\xi)}{d\xi} + h'(U_0(\xi))B(\xi) + F'(U_0(\xi)) \int_{-\infty}^{\infty} w(\xi - \xi')B(\xi')d\xi'. \quad (2.23)$$

It can be proven that  $\widehat{L}^*$  also has a one-dimensional null-space [20], that is, it is spanned by some function  $\mathcal{V}(\xi)$ . Thus taking the inner product of both sides of equation (2.20) with respect to  $\mathcal{V}(\xi)$  leads to the solvability condition

$$\int_{-\infty}^{\infty} \mathcal{V}(\xi) \left[ U_0'(\xi)d\Delta(t) + \varepsilon^{1/2}dR(U_0, \xi, t) \right] d\xi = 0. \quad (2.24)$$

Thus  $\Delta(t)$  satisfies the stochastic differential equation (SDE)

$$d\Delta(t) = -\varepsilon^{1/2} \frac{\int_{-\infty}^{\infty} \mathcal{V}(\xi)dR(U_0, \xi, t)d\xi}{\int_{-\infty}^{\infty} \mathcal{V}(\xi)U_0'(\xi)d\xi}. \quad (2.25)$$

Using the lowest order approximation  $dR(U_0, \xi, t) = g(U_0(\xi))dW(\xi, t)$ , we deduce that (for  $\Delta(0) = 0$ )

$$\langle \Delta(t) \rangle = 0, \quad \langle \Delta(t)^2 \rangle = 2D(\varepsilon)t \quad (2.26)$$

where  $D(\varepsilon)$  is the the effective diffusivity

$$\begin{aligned} D(\varepsilon) &= \varepsilon \frac{\int_{-\infty}^{\infty} \int_{-\infty}^{\infty} \mathcal{V}(\xi)\mathcal{V}(\xi')g(U_0(\xi))g(U_0(\xi'))\langle dW(\xi, t)dW(\xi', t) \rangle d\xi d\xi'}{\left[ \int_{-\infty}^{\infty} \mathcal{V}(\xi)U_0'(\xi)d\xi \right]^2} \\ &= \varepsilon \frac{\int_{-\infty}^{\infty} \mathcal{V}(\xi)^2 g^2(U_0(\xi))d\xi}{\left[ \int_{-\infty}^{\infty} \mathcal{V}(\xi)U_0'(\xi)d\xi \right]^2}. \end{aligned} \quad (2.27)$$

**2.3. Explicit results for Heaviside rate function.** We now illustrate the above analysis by considering a particular example where the mean speed  $c_\varepsilon$  and diffusion coefficient  $D(\varepsilon)$  can be calculated explicitly. That is, we take  $g(U) = g_0U$  for the multiplicative noise term and set  $F(U) = H(U - \kappa)$ . (The constant  $g_0$  has units of  $\sqrt{\text{length}/\text{time}}$ ). The deterministic equation (2.19) for the mean profile  $U_0$  then reduces to

$$-c_\varepsilon \frac{dU_0}{d\xi} + U_0(\xi)[1 - \varepsilon g_0^2 C(0)] = \int_{-\infty}^{\infty} w(\xi - \xi')H(U_0(\xi') - \kappa)d\xi'. \quad (2.28)$$

This is identical in structure to equation (2.6) for the deterministic neural field modulo the rescaling of the decay term. The analysis of the wave speeds proceeds as in section 2.1 and we find that for  $c_\varepsilon > 0$ ,

$$c_\varepsilon = \gamma(\varepsilon)c_+ + (\gamma(\varepsilon)\kappa) = \frac{\sigma}{2\kappa}[1 - 2\kappa\gamma(\varepsilon)], \quad (2.29)$$

whereas, for  $c_\varepsilon < 0$ ,

$$c_\varepsilon = \gamma(\varepsilon)c_+(\gamma(\varepsilon)\kappa) = \frac{\sigma\gamma(\varepsilon)}{2} \frac{1 - 2\kappa\gamma(\varepsilon)}{1 - \kappa\gamma(\varepsilon)}, \quad (2.30)$$

with

$$\gamma(\varepsilon) = (1 - \varepsilon g_0^2 C(0)), \quad (2.31)$$

and  $c_\pm(\kappa)$  defined in equation (2.10). Assuming that  $0 \leq \gamma(\varepsilon) \leq 1$ , we see that multiplicative noise shifts the mean velocity of front propagation in the positive  $\xi$  direction.

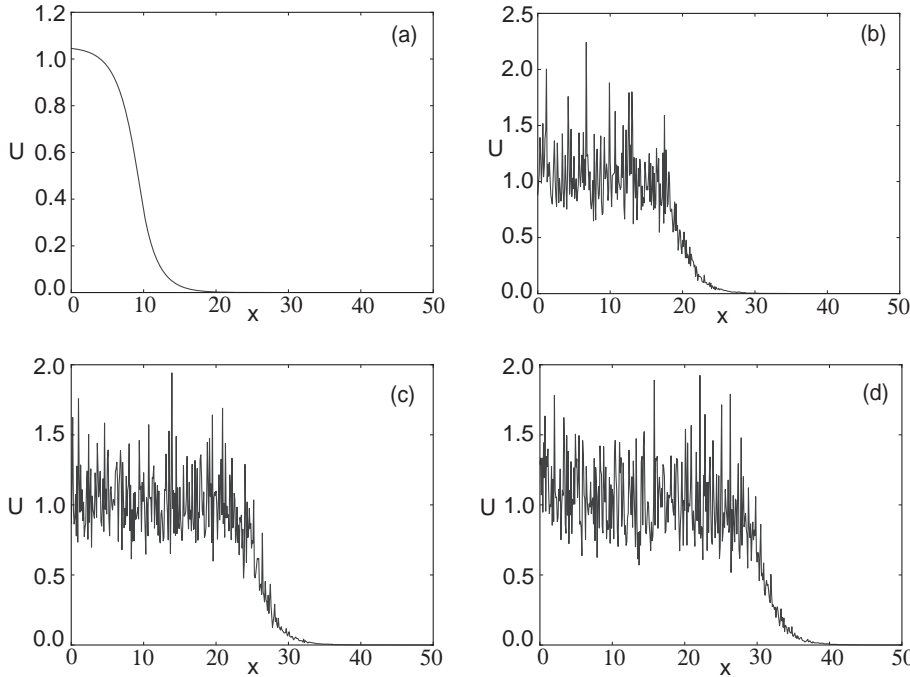


FIG. 2.1. Numerical simulation showing the propagation of a front solution of the stochastic neural field equation (2.11) for Heaviside weight function  $F(U) = H(U - \kappa)$  with  $\kappa = 0.35$ , exponential weight function (2.4) with  $\sigma = 2$ , and multiplicative noise  $g(U) = U$ . Noise strength  $\varepsilon = 0.005$  and  $C(0) = 10$ . The wave profile is shown at successive times (a)  $t = 0$  (b)  $t = 12$  (c)  $t = 18$  and (d)  $t = 24$ , with the initial profile at  $t = 0$  given by equation (2.34). In numerical simulations we take the discrete space and time steps  $\Delta x = 0.1, \Delta t = 0.01$ .

In order to calculate the diffusion coefficient, it is first necessary to determine the null vector  $\mathcal{V}(\xi)$  of the adjoint linear operator  $\tilde{L}^*$  defined by equation (2.23). Setting  $F(U) = H(U - \kappa)$  and  $g(U) = g_0 U$ , the null vector  $\mathcal{V}$  satisfies the equation

$$c_\varepsilon \mathcal{V}'(\xi) + [1 - \varepsilon g_0^2 C(0)] \mathcal{V}(\xi) = -\frac{\delta(\xi)}{U'_0(0)} \int_{-\infty}^{\infty} w(\xi') \mathcal{V}(\xi') d\xi'. \quad (2.32)$$

This can be solved explicitly to give [7]

$$\mathcal{V}(\xi) = -H(\xi) \exp(-\Gamma(\varepsilon)\xi), \quad \Gamma(\varepsilon) = \frac{\gamma(\varepsilon)}{c_\varepsilon}. \quad (2.33)$$

We have used the fact that the solution to equation (2.28) is of the form

$$U_0(\xi) = \frac{1}{c_\varepsilon} \int_0^\infty e^{-\Gamma(\varepsilon)y} W(y + \xi) dy, \quad (2.34)$$

with  $W(\xi)$  defined in equation (2.6) and, hence,

$$U'_0(\xi) = -\frac{1}{c_\varepsilon} \int_0^\infty e^{-\Gamma(\varepsilon)y} w(y + \xi) dy. \quad (2.35)$$

In the case of an exponential weight distribution,  $U_0(\xi)$  can be evaluated explicitly to give

$$U_0(\xi) = \begin{cases} \frac{1}{2c_\varepsilon} \frac{\sigma e^{-\xi/\sigma}}{1 + \sigma\Gamma(\varepsilon)} & \xi \geq 0 \\ \frac{1}{2c_\varepsilon} \left[ \frac{2e^{\xi\Gamma(\varepsilon)}}{\Gamma(\varepsilon)(-1 + \sigma^2\Gamma(\varepsilon)^2)} + \frac{2}{\Gamma(\varepsilon)} + \frac{\sigma e^{\xi/\sigma}}{1 - \sigma\Gamma(\varepsilon)} \right] & \xi < 0. \end{cases} \quad (2.36)$$

Using equation (2.33), equation (2.27) reduces to the form

$$D(\varepsilon) = \varepsilon \frac{\int_0^\infty e^{-2\Gamma(\varepsilon)\xi} U_0(\xi)^2 d\xi}{\left[ \int_0^\infty e^{-\Gamma(\varepsilon)\xi} U'_0(\xi) d\xi \right]^2}. \quad (2.37)$$

which can be evaluated explicitly using equation (2.36) to obtain

$$D(\varepsilon) = \frac{1}{2} \varepsilon \sigma g_0^2 (1 + \sigma\Gamma(\varepsilon)) \quad (2.38)$$

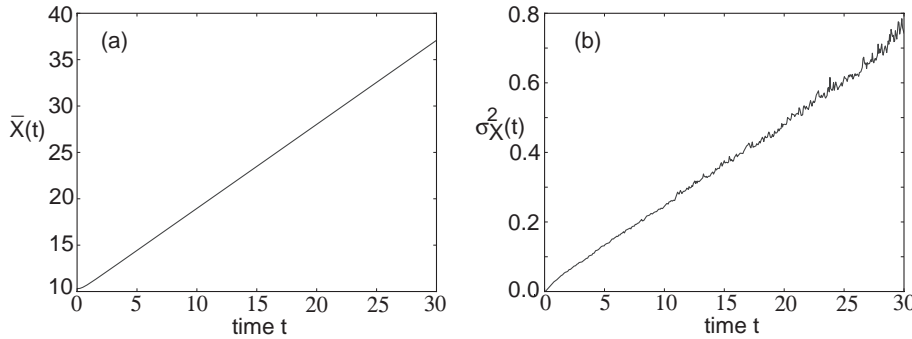


FIG. 2.2. Plot of (a) mean  $\bar{X}(t)$  and (b) variance  $\sigma_X^2(t)$  of front position as a function of time, averaged over  $N = 4096$  trials. Same parameter values as Fig. 2.1

In Fig. 2.1 we show the temporal evolution of a single stochastic wave front, which is obtained by numerically solving the Langevin equation (2.11) for  $F(U) = H(U - \kappa)$ ,  $g(U) = U$  and an exponential weight distribution  $w$ . In order to numerically calculate the mean location of the front as a function of time, we carry out a large number of level set position measurements. That is, we determine the positions  $X_a(t)$  such that  $U(X_a(t), t) = a$ , for various level set values  $a \in (0.5\kappa, 1.3\kappa)$  and then define the mean

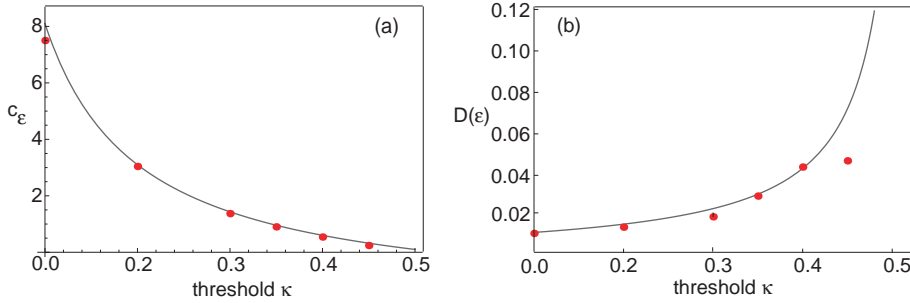


FIG. 2.3. Plot of (a) wave speed  $c_\varepsilon$  and (b) diffusion coefficient  $D(\varepsilon)$  as a function of threshold  $\kappa$ . Numerical results (solid dots) are obtained by averaging over  $N = 4096$  trials starting from the initial condition given by Eq. (2.34). Corresponding theoretical predictions (solid curves) for  $c_\varepsilon$  and  $D(\varepsilon)$  are based on equations (2.29) and (2.37), respectively. Other parameters as in Fig. 2.1.

location to be  $\bar{X}(t) = \mathbb{E}[X_a(t)]$ , where the expectation is first taken with respect to the sampled values  $a$  and then averaged over  $N$  trials. The corresponding variance is given by  $\sigma_X^2(t) = \mathbb{E}[(X_a(t) - \bar{X}(t))^2]$ . In Fig. 2.2 we plot  $\bar{X}(t)$  and  $\sigma_X^2(t)$  as a function of  $t$ . It can be seen that both vary linearly with  $t$ , consistent with the assumption that there is a diffusive-like displacement of the front from its uniformly translating position at long time scales. The slopes of these curves then determine the effective wave speed and diffusion coefficient according to  $\bar{X}(t) \sim c_\varepsilon t$  and  $\sigma_X^2(t) \sim 2D(\varepsilon)t$ . In Fig. 2.3 we plot the numerically estimated speed and diffusion coefficient for various values of the threshold  $\kappa$  and compare these to the corresponding theoretical curves obtained using the above analysis. It can be seen that there is excellent agreement with our theoretical predictions provided that  $\kappa$  is not too large. As  $\kappa \rightarrow 0.5$ , the wave speed decreases towards zero so that the assumption of relatively slow diffusion breaks down.

### 3. Effects of multiplicative noise on stimulus-locked fronts.

**3.1. Stimulus-locked fronts.** So far we have assumed that the underlying deterministic neural field equation is homogeneous in space so that there exists a family of traveling front solutions related by a uniform shift. Now suppose that there exists an external front-like input that propagates at a uniform speed  $v$ , so that the deterministic equation (2.1) becomes

$$\frac{\partial u(x, t)}{\partial t} = -u(x, t) + \int_{-\infty}^{\infty} w(x - x') F(u(x', t)) dx' + I(x - vt), \quad (3.1)$$

where the input is taken to be a positive, bounded, monotonically decreasing function of amplitude  $I_0 = I(-\infty) - I(\infty)$ . Previously we have shown that the resulting inhomogeneous neural field equation can support a traveling front that locks to the stimulus, provided that the amplitude of the stimulus is sufficiently large [25]. Consider, in particular, the case of a Heaviside firing rate function  $F(u) = H(u - \kappa)$ . (See [22] for a recent extension to the case of a smooth sigmoid function  $F$ ). We seek a traveling wave solution  $u(x, t) = \mathcal{U}(\xi)$  where  $\xi = x - vt$  and  $\mathcal{U}(\xi_0) = \kappa$  at a single threshold crossing point  $\xi_0 \in \mathbb{R}$ . The front is assumed to travel at the same speed as the input (stimulus-locked front). If  $I_0 = 0$  then we recover the homogeneous equation (2.1) and  $\xi_0$  becomes a free parameter, whereas the wave propagates at the natural speed  $c(\kappa)$  given by equation (2.10). Substituting the front solution

into equation (3.1), we have

$$-v \frac{d\mathcal{U}(\xi)}{d\xi} = -\mathcal{U}(\xi) + \int_{-\infty}^{\xi_0} w(\xi - \xi') d\xi' + I(\xi). \quad (3.2)$$

This can be solved for  $v > 0$  by integrating over the interval  $[\xi, \infty)$  to give

$$\mathcal{U}(\xi) = \frac{1}{v} \int_{\xi}^{\infty} e^{(\xi - \xi')/v} [W(\xi' - \xi_0) + I(\xi')] d\xi',$$

with  $W(\xi)$  defined according to equation (2.6). Similarly, for  $v < 0$  we integrate over  $(-\infty, \xi]$  to find

$$\mathcal{U}(\xi) = -\frac{1}{v} \int_{-\infty}^{\xi} e^{(\xi - \xi')/v} [W(\xi' - \xi_0) + I(\xi')] d\xi'.$$

The threshold crossing condition  $\mathcal{U}(\xi_0) = \kappa$  then determines the position  $\xi_0$  of the front relative to the input as a function of speed  $v$ , input amplitude  $I_0$  and threshold  $\kappa$ .

As a specific example, suppose that  $I(\zeta) = I_0 H(-\zeta)$  and  $w(x)$  is the exponential weight distribution (2.4). The threshold condition reduces to

$$\kappa = \begin{cases} \frac{\sigma}{2(\sigma + v)} + \begin{cases} 0, & \xi_0 \geq 0, \\ I_0(1 - e^{\xi_0/v}), & \xi_0 < 0, \end{cases} & v > 0; \\ \frac{\sigma + 2|v|}{2(\sigma + |v|)} + \begin{cases} I_0 e^{\xi_0/v}, & \xi_0 > 0, \\ I_0, & \xi_0 \leq 0, \end{cases} & v < 0. \end{cases} \quad (3.3)$$

Note that in the absence of any input ( $I_0 = 0$ ), we recover equation (2.10) with  $v \rightarrow c(\kappa)$ , the natural wave speed. Equation (3.3) for  $I_0 > 0$  can then be used to determine the regions of the  $(v, I_0)$ -parameter subspace for which stimulus-locked waves exist. Let us first consider the case  $v > 0$ . If  $\xi_0 \geq 0$  then  $\kappa = \sigma/[2(\sigma + v)]$ , which implies that stimulus locking only occurs when the input speed equals the natural wave speed, that is,  $v = c_+(\kappa)$  for  $0 < \kappa < \frac{1}{2}$  and  $\xi_0 > 0$ . There are infinitely many such waves, which are parameterized by  $\xi_0 \in [0, \infty)$ . This degeneracy is a consequence of using the Heaviside input and would not occur, if a continuous, strictly monotonic input were used; however, the analysis is considerably more involved [22]. On the other hand, if  $\xi_0 < 0$  then  $\kappa = \sigma/[2(\sigma + v)] + I_0(1 - e^{\xi_0/v})$ , which can be inverted to solve for  $\xi_0$  as a function of  $v$ :

$$\xi_0(v) = v \ln \left[ 1 - \frac{1}{I_0} \left( \kappa - \frac{\sigma}{2(\sigma + v)} \right) \right].$$

Since  $\xi_0 < 0$  and  $v > 0$ , it follows that solutions only exist if

$$2(\kappa - I_0) < \frac{\sigma}{\sigma + v} \leq 2\kappa. \quad (3.4)$$

The right inequality of (3.4) implies that, if  $\kappa < \frac{1}{2}$ , then  $v > c_+(\kappa)$  where  $c_+(\kappa)$  is the wavespeed of freely propagating fronts, see equation (2.10). Similarly, the left

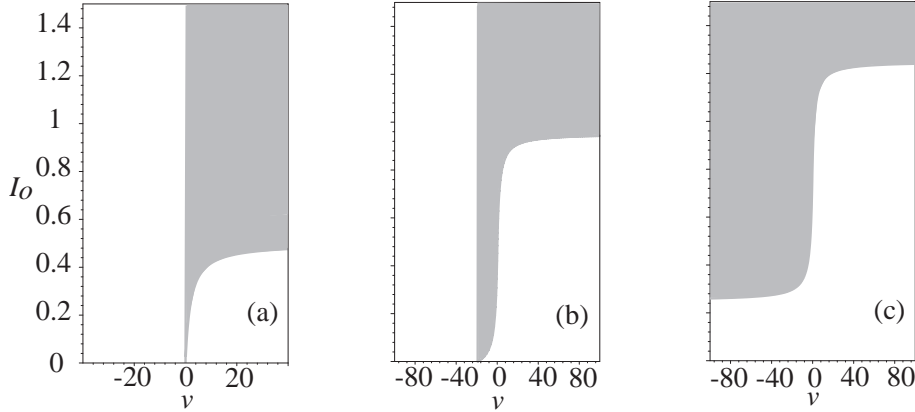


FIG. 3.1. Existence regions for stimulus-locked traveling fronts in the  $(I_0, v)$ -plane (gray) for various thresholds  $\kappa$ : (a)  $\kappa = 0.5$ , (b)  $\kappa = 0.95$ , (c)  $\kappa = 1.25$ .

inequality implies that, if  $I_0 < \kappa$ , then  $0 < v < c_+(\kappa - I_0)$ . Hence, for  $0 < \kappa \leq \frac{1}{2}$  we obtain the existence regions in the  $(v, I_0)$ -plane shown in Fig. 3.1(a). The left boundary is given by  $v = c_+(\kappa)$  and the right boundary by  $v = c_+(\kappa - I_0)$ . The two boundaries form a tongue that emerges from the natural speed  $c_+(\kappa)$  at  $I_0 = 0$ .

Now consider the case  $v < 0$ . For  $\xi_0 < 0$  we have the threshold condition  $\kappa = (\sigma + 2|v|)/(2(\sigma + |v|)) + I_0$ , which implies that  $v = c_-(\kappa - I_0) < 0$ . Again we have an infinite family of waves corresponding to a single speed. Since  $|v| \geq 0$ , such solutions only exist for  $\kappa - 1 < I_0 < \kappa - 1/2$ . On the other hand, for  $\xi_0 \geq 0$  we have the threshold condition  $\kappa = (\sigma + 2|v|)/(2(\sigma + |v|)) + I_0 e^{\xi_0/v}$ , which can be inverted to give

$$\xi_0(v) = v \ln \left[ \frac{1}{I_0} \left( \kappa - \frac{\sigma + 2|v|}{2(\sigma + |v|)} \right) \right].$$

Since  $v < 0$  and  $\xi_0 \geq 0$ , it follows that waves only exist for  $v$  satisfying

$$\kappa - I_0 \leq \frac{\sigma + 2|v|}{2(\sigma + |v|)} < \kappa. \quad (3.5)$$

The right inequality of (3.5) implies that, if  $\frac{1}{2} < \kappa < 1$ , then  $c_-(\kappa) < v < 0$ . Thus, for  $1/2 < \kappa < 1$  we obtain the existence region shown in figure 3.1(b); the left boundary is given by  $v = c_-(\kappa)$  and the right boundary by  $v = c_-(\kappa - I_0)$  for  $v < 0$  and  $v = c_+(\kappa - I_0)$  for  $v > 0$ . Again there is a tongue with tip at the natural speed. For  $\kappa > 1$  the left boundary disappears, and one only finds stimulus-locked waves when  $I_0 > \kappa - 1$ , i.e., there no longer exists natural waves. The left inequality of (3.5) implies that if  $1/2 < \kappa - I_0 < 1$  then  $v < c_-(\kappa - I_0) < 0$ , whereas, if  $\kappa - I_0 > 1$  then no solution exists, see Fig. 3.1(c).

**3.2. Locking in the presence of multiplicative noise.** We now extend the analysis of section 2 in order to determine the effects of multiplicative noise on stimulus-locked fronts, and show that diffusive-like behavior found for freely propagating fronts no longer holds. Incorporating the external input into the Langevin

equation (2.11) gives

$$dU(x, t) = \left[ -U(x, t) + \int_{-\infty}^{\infty} w(x-y)F(U(y, t))dy + I(x-vt) \right] dt + \varepsilon^{1/2}g(U(x, t))dW(x, t). \quad (3.6)$$

Applying equation (2.13), we then rewrite equation (3.6) so that the fluctuating term has zero mean:

$$dU(x, t) = \left[ h(U(x, t)) + \int_{-\infty}^{\infty} w(x-y)F(U(y, t))dy + I(x-vt) \right] dt + \varepsilon^{1/2}dR(U, x, t), \quad (3.7)$$

where  $h$  and  $R$  are given by equations (2.15) and (2.16), respectively. Proceeding along similar lines to our analysis of freely propagating fronts, we express the solution  $U$  of equation (3.7) as a combination of a fixed wave profile  $U_0$  that is displaced by an amount  $\Delta(t)$  from its uniformly translating mean position  $\xi = x - vt$ , and a time-dependent fluctuation  $\Phi$  in the front shape about the instantaneous position of the front:

$$U(x, t) = U_0(\xi - \Delta(t)) + \varepsilon^{1/2}\Phi(\xi - \Delta(t), t). \quad (3.8)$$

We are assuming that the mean profile  $U_0$  is locked to the stimulus (has speed  $v$ ). However, multiplicative noise still has an effect on  $U_0$  by generating an  $\varepsilon$ -dependent threshold crossing point  $\xi_\varepsilon$  such that  $U_0(\xi_\varepsilon) = \kappa$ .

Substituting equation (3.8) into equation (3.7) and taking averages gives to leading order the following deterministic equation for  $U_0$ :

$$-v \frac{dU_0}{d\xi} - h(U_0(\xi)) - I(\xi) = \int_{-\infty}^{\infty} w(\xi - \xi')F(U_0(\xi'))d\xi'. \quad (3.9)$$

Note that  $U_0$  depends non-trivially on the noise strength  $\varepsilon$  due to the  $\varepsilon$ -dependence of the function  $h$ , see equation (2.15). Proceeding to the next order and imposing equation (3.9), we find that  $\Delta(t) = \mathcal{O}(\varepsilon^{1/2})$  and

$$d\Phi(\xi, t) = \widehat{L} \circ \Phi(\xi, t)dt + \varepsilon^{-1/2}U_0'(\xi)d\Delta(t) + dR(U_0, \xi, t) + \varepsilon^{-1/2}I'(\xi)\Delta(t)dt \quad (3.10)$$

where  $\widehat{L}$  is the non-self-adjoint linear operator (2.21) with  $c_\varepsilon \rightarrow v$ . The last term on the right-hand side of equation (3.10) arises from the fact that in equation (3.8),  $U_0$  and  $\Phi$  are expressed as functions of  $\xi - \Delta(t)$  so that we have made the approximation  $I(\xi) = I(\xi - \Delta(t) + \Delta(t)) \approx I(\xi - \Delta(t)) + I'(\xi - \Delta(t))\Delta(t)$ . We then have the solvability condition for the existence of a nontrivial solution of equation (3.10), namely, that the inhomogeneous part is orthogonal to the null vector  $\mathcal{V}(\xi)$  of the adjoint operator  $\widehat{L}^*$  defined by equation (2.23) with  $c_\varepsilon \rightarrow v$ . Taking the inner product of both sides of equation (3.10) with respect to  $\mathcal{V}(\xi)$  thus leads to the solvability condition

$$\int_{-\infty}^{\infty} \mathcal{V}(\xi) \left[ U_0'(\xi)d\Delta(t) + I'(\xi)\Delta(t)dt + \varepsilon^{1/2}dR(U_0, \xi, t) \right] d\xi = 0. \quad (3.11)$$

It follows that, to leading order,  $\Delta(t)$  satisfies the Ornstein-Uhlenbeck equation

$$d\Delta(t) + A\Delta(t)dt = d\widehat{W}(t), \quad (3.12)$$

where

$$A = \frac{\int_{-\infty}^{\infty} \nu(\xi) I'(\xi) d\xi}{\int_{-\infty}^{\infty} \nu(\xi) U_0'(\xi) d\xi}. \quad (3.13)$$

and

$$\widehat{W}(t) = -\varepsilon^{1/2} \frac{\int_{-\infty}^{\infty} \nu(\xi) g(U_0(\xi)) W(\xi, t) d\xi}{\int_{-\infty}^{\infty} \nu(\xi) U_0'(\xi) d\xi}. \quad (3.14)$$

Note that  $A > 0$  for  $I_0 > 0$ , since both  $U_0(\xi)$  and  $I(\xi)$  are monotonically decreasing functions of  $\xi$ . Moreover

$$\langle d\widehat{W}(t) \rangle = 0, \quad \langle d\widehat{W}(t) d\widehat{W}(t) \rangle = 2D(\varepsilon) dt \quad (3.15)$$

with  $D(\varepsilon)$  given by equation (2.27). Using standard properties of an Ornstein-Uhlenbeck process [27], we conclude that

$$\langle \Delta(t) \rangle = \Delta(0) e^{-At}, \quad \langle \Delta(t)^2 \rangle - \langle \Delta(t) \rangle^2 = \frac{D(\varepsilon)}{A} [1 - e^{-2At}]. \quad (3.16)$$

In particular, the variance approaches a constant  $D(\varepsilon)/A$  in the large  $t$  limit.

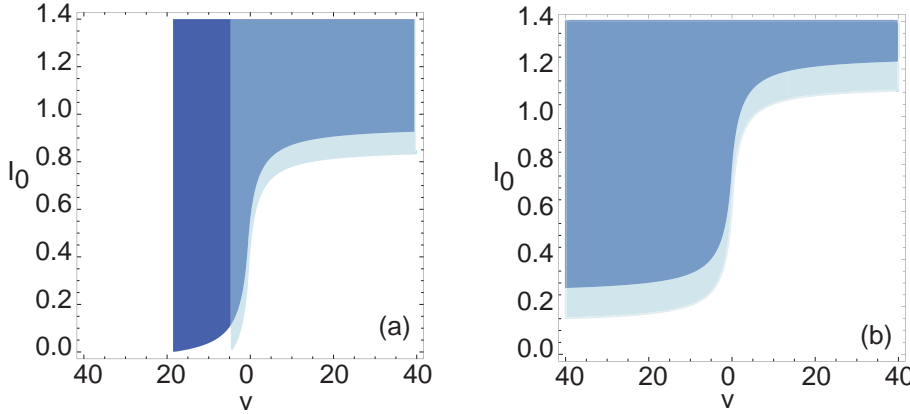


FIG. 3.2. Plot of existence regions of a stimulus-locked front without noise ( $\gamma = 1$ , dark blue) and in the presence of noise ( $\gamma = 0.9$ , light blue) for a)  $\kappa = 0.95$  b)  $\kappa = 1.25$ . Stimulus taken to be of the form  $I(x, t) = I_0 H(-\xi)$ ,  $\xi = x - vt$  with amplitude  $I_0$  and speed  $v$ . Other parameter values as in Fig. 2.1.

**3.3. Heaviside rate function.** In order to illustrate the above analysis, we take  $g(U) = g_0 U$  for the multiplicative noise term and set  $F(U) = H(U - \kappa)$ . The deterministic equation (3.9) for the mean profile  $U_0$  then reduces to

$$-v \frac{dU_0}{d\xi} + U_0(\xi) [1 - \varepsilon g_0^2 C(0)] + I(\xi) = \int_{-\infty}^{\infty} w(\xi - \xi') H(U_0(\xi') - \kappa) d\xi'. \quad (3.17)$$

Proceeding as in §3.1, we can explicitly calculate the existence regions for stimulus locked fronts when  $I(\xi) = I_0 H(-\xi)$ , that is, for a step function input of speed  $v$  and amplitude  $I_0$ . Setting  $\gamma(\varepsilon) = 1 - \varepsilon g_0^2 C(0)$  with  $0 < \gamma(\varepsilon) \leq 1$ , and introducing the threshold crossing point  $\xi_\varepsilon$  for which  $U_0(\xi_\varepsilon) = \kappa$ , we derive a similar set of threshold conditions as equation (3.3) under the rescalings  $\kappa \rightarrow \eta\gamma(\varepsilon)$  and  $v \rightarrow v/\gamma(\varepsilon)$ :

$$\gamma(\varepsilon)\kappa = \begin{cases} \frac{\sigma}{2(\sigma + v/\gamma(\varepsilon))} + \begin{cases} 0, & \xi_0 \geq 0, \\ I_0(1 - e^{\gamma(\varepsilon)\xi_0/v}), & \xi_0 < 0, \end{cases} & v > 0; \\ \frac{\sigma + 2|v|/\gamma(\varepsilon)}{2(\sigma + |v|/\gamma(\varepsilon))} + \begin{cases} I_0 e^{\gamma(\varepsilon)\xi_0/v}, & \xi_0 > 0, \\ I_0, & \xi_0 \leq 0, \end{cases} & v < 0. \end{cases} \quad (3.18)$$

It follows that the boundaries of the existence tongues are now determined by the modified functions  $\gamma(\varepsilon)c_\pm(\gamma(\varepsilon)\kappa - I_0)$ . The resulting  $\varepsilon$ -dependent shift in the existence tongues is illustrated in Fig. 3.2.

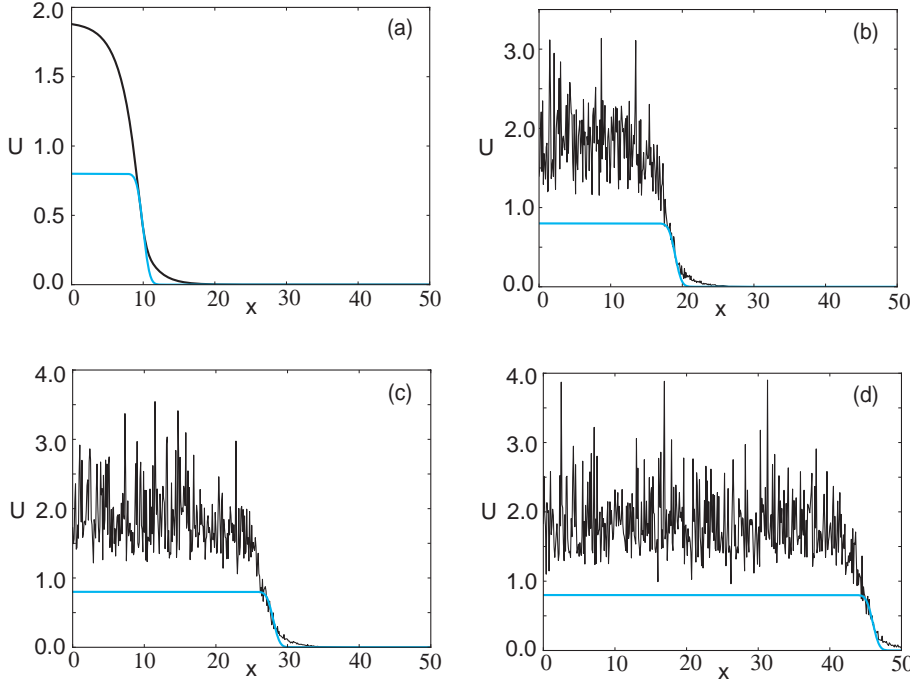


FIG. 3.3. Numerical simulation showing the propagation of a stimulus-locked wavefront solution (black curves) of the stochastic neural field equation (3.6) for Heaviside weight function  $F(U) = H(U - \kappa)$  with  $\kappa = 0.35$ , exponential weight function (2.4) with  $\sigma = 2$ , and multiplicative noise  $g(U) = U$ . The external input (light blue curves) is taken to be of the form  $I(x, t) = I_0 \text{Erfc}[x - vt]$  with amplitude  $I_0 = 0.4$  and speed  $v = 1.5$ . Noise strength  $\varepsilon = 0.005$  and  $C(0) = 10$ . The wave profile is shown at successive times (a)  $t = 0$  (b)  $t = 6$  (c)  $t = 12$  and (d)  $t = 24$ , with the initial profile at  $t = 0$  given by the solution  $U_0$  of equation (3.9). In numerical simulations we take the discrete space and time steps  $\Delta x = 0.1, \Delta t = 0.01$ .

In Fig. 3.3 we show the temporal evolution of a single stimulus-locked front, which

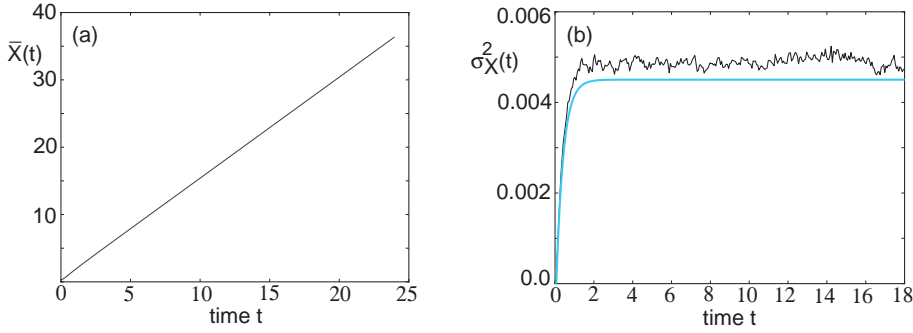


FIG. 3.4. Plot of (a) mean  $\bar{X}(t)$  and (b) variance  $\sigma_X^2(t)$  of the position of a stimulus-locked front as a function of time, averaged over  $N = 4096$  trials. Smooth blue curve in (b) indicates theoretical prediction of variance. Stimulus taken to be of the form  $I(x, t) = I(x - ct) = I_0 \text{Erfc}[x - vt]$  with amplitude  $I_0 = 0.4$  and speed  $v = 1.5$ . Other parameter values as in Fig. 2.1 and initial condition satisfying equation (2.34).

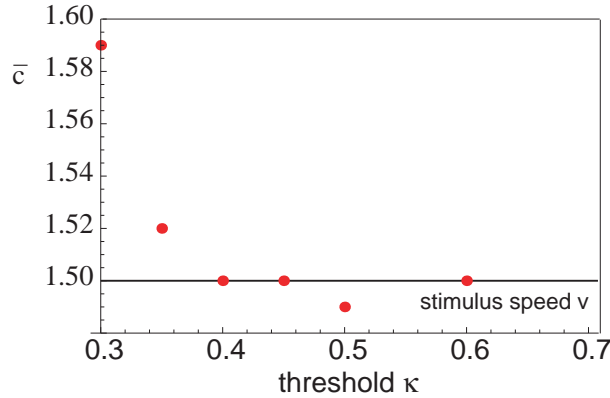


FIG. 3.5. Plot of mean wave speed  $\bar{c}$  as a function of threshold  $\kappa$ . Other parameters as in Fig. 3.4. Horizontal curve indicates speed  $v$  of stimulus. Stimulus-locked waves do not exist for  $\kappa < 0.30$  which explains why the datapoint at  $\kappa = 0.30$  is an outlier.

is obtained by numerically solving the Langevin equation (3.6) for  $F(U) = H(U - \kappa)$ ,  $g(U) = U$  and an exponential weight distribution  $w$ . Numerically speaking, it is convenient to avoid discontinuities in the input by taking  $I(x, t) = I_0 \text{Erfc}[x - vt]$  rather than a Heaviside. Next we determine the mean  $\bar{X}(t)$  and variance  $\sigma_X^2(t)$  of the position of the front by averaging over level sets along identical lines to §2.3. The results are shown in Fig. 3.4. It can be seen that, as predicted by the analysis,  $\bar{X}(t)$  varies linearly with  $t$  with a slope equal to the stimulus speed  $v = 1.5$ . Moreover, the variance  $\sigma_X^2(t)$  approaches a constant value as  $t \rightarrow \infty$ , which is comparable to the theoretical value  $D(\varepsilon)/A$  evaluated for the given input. Thus, we find that stimulus-locked fronts are much more robust to noise than freely propagating fronts, since the variance of the mean position saturates as  $t \rightarrow \infty$ . Consequently, stimulus locking persists in the presence of noise over most of the parameter range for which stimulus locking is predicted to occur. This is further illustrated in Fig. 3.5, where we plot the mean speed of the wave as a function of the threshold  $\kappa$ .

**4. Neural fields and pulled fronts.** Neural field equations with a sigmoidal or Heaviside nonlinearity tend to support a pair of stable spatially uniform fixed points (corresponding to low and high activity states, respectively) so that a front solution linking these states propagates into a (meta)stable state rather than an unstable state. However, it is possible to construct a neural field equation in which the low activity state is unstable. Consider, for example, the model

$$\tau \frac{\partial a(x, t)}{\partial t} = -a(x, t) + F \left( \int_{-\infty}^{\infty} w(x - x') a(x', t) dx' \right). \quad (4.1)$$

In contrast to equation (2.1), in which  $u(x, t)$  represents a local population current or voltage, the field  $a(x, t)$  represents a local population firing rate. (For a detailed discussion of different neural field representations see the reviews [21, 11]). In addition to the convolution integral now being inside the nonlinear rate function  $F$ , we have the additional constraint that  $a(x, t) \geq 0$  for all  $(x, t)$ . Note that the restriction to positive values of  $a$  is a feature shared with population models in ecology or evolutionary biology, for example, where the corresponding dependent variables represent number densities. Indeed, equation (4.1) has certain similarities with a nonlocal version of the Fisher-Kolmogorov *et. al.* (F-KPP) equation, which takes the form [28, 4]

$$\tau \frac{\partial p(x, t)}{\partial t} = D \frac{\partial^2 p(x, t)}{\partial x^2} + \mu p(x, t) \left( 1 - \int_{-\infty}^{\infty} K(x - x') p(x', t) dx' \right). \quad (4.2)$$

One major difference from a mathematical perspective is that equation (4.2) supports traveling fronts even when the range of the interaction kernel  $K$  goes to zero, that is,  $K(x) \rightarrow \delta(x)$ , since we recover the standard local F-KPP equation [24, 32]. In particular, as the nonlocal interactions appear nonlinearly in equation (4.2) they do not contribute to the linear spreading velocity in the leading edge of the front. On the other hand, nonlocal interactions play a necessary role in the generation of fronts in the neural field equation (4.1).

**4.1. Wave speed and asymptotic convergence.** Suppose that  $F(a)$  in equation (4.1) is a positive, bounded, monotonically increasing function of  $a$  with  $F(0) = 0$ ,  $\lim_{a \rightarrow 0^+} F'(a) = 1$  and  $\lim_{a \rightarrow \infty} F(a) = 1$ . For concreteness, we take

$$F(a) = \begin{cases} 0, & a \leq 0 \\ a, & 0 < a \leq \kappa \\ \kappa, & a > \kappa. \end{cases} \quad (4.3)$$

A homogeneous fixed point solution  $A^*$  of equation (4.1) satisfies

$$A^* = F(W_0 A^*), \quad W_0 = \int_{-\infty}^{\infty} w(y) dy. \quad (4.4)$$

In the case of the given piecewise linear firing rate function, we find that if  $W_0 > 1$ , then there exists an unstable fixed point at  $A^* = 0$  and a stable fixed point at  $A^* = \kappa$ . The construction of a front solution linking the stable and unstable fixed points differs considerably from that considered in §2. Following the PDE theory of fronts propagating into unstable states [46], we expect there to be a continuum of front velocities and associated traveling wave solutions. A conceptual framework for studying such solutions is the linear spreading velocity  $v^*$ , which is the asymptotic rate with which an initial localized perturbation spreads into an unstable state based

on the linear equations obtained by linearizing the full nonlinear equations about the unstable state. Thus, consider a traveling wave solution  $\mathcal{A}(x - ct)$  of equation (4.1) with  $\mathcal{A}(\xi) \rightarrow \kappa$  as  $\xi \rightarrow -\infty$  and  $\mathcal{A}(\xi) \rightarrow 0$  as  $\xi \rightarrow \infty$ . One can determine the range of velocities  $c$  for which such a solution exists by assuming that  $\mathcal{A}(\xi) \approx e^{-\lambda\xi}$  for sufficiently large  $\xi$ . The exponential decay of the front suggests that we linearize equation (4.1), which in traveling wave coordinates (with  $\tau = 1$ ) takes the form

$$-c \frac{d\mathcal{A}(\xi)}{d\xi} = -\mathcal{A}(\xi) + \int_{-\infty}^{\infty} w(\xi - \xi') \mathcal{A}(\xi') d\xi'. \quad (4.5)$$

However, in order to make the substitution  $\mathcal{A}(\xi) \approx e^{-\lambda\xi}$  we need to restrict the integration domain of  $\xi'$  to the leading edge of the front. Suppose, for example that  $w(x)$  is given by the Gaussian distribution

$$w(x) = \frac{W_0}{\sqrt{2\pi\sigma^2}} e^{-x^2/2\sigma^2}. \quad (4.6)$$

Given the fact that the front solution  $\mathcal{A}(\xi)$  is bounded, we introduce a cut-off  $X$  with  $\sigma \ll X \ll \xi$ , and approximate equation (4.5) by

$$-c \frac{d\mathcal{A}(\xi)}{d\xi} = -\mathcal{A}(\xi) + \int_{\xi-X}^{\xi+X} w(\xi - \xi') \mathcal{A}(\xi') d\xi'. \quad (4.7)$$

Substituting the exponential solution in (4.5) then yields the dispersion relation  $c = c(\lambda)$  with

$$c(\lambda) = \frac{1}{\lambda} \left[ \int_{-X}^X w(y) e^{-\lambda y} dy - 1 \right]. \quad (4.8)$$

Finally, we now take the limit  $X \rightarrow \infty$  under the assumption that  $w(y)$  is an even function to yield

$$c(\lambda) = \frac{1}{\lambda} \left[ \widehat{W}(\lambda) + \widehat{W}(-\lambda) - 1 \right], \quad (4.9)$$

where  $\widehat{W}(\lambda)$  is the Laplace transform of  $w(x)$ :

$$\widehat{W}(\lambda) = \int_0^{\infty} w(y) e^{-\lambda y} dy. \quad (4.10)$$

If  $W_0 > 1$  (necessary for the zero activity state to be unstable) then  $c(\lambda)$  is a positive unimodal function with  $c(\lambda) \rightarrow \infty$  as  $\lambda \rightarrow 0$  or  $\lambda \rightarrow \infty$  and a unique minimum at  $\lambda = \lambda^*$ , see black curve in Fig. 4.1. Assuming that the full nonlinear system supports a pulled front then a sufficiently localized initial perturbation (one that decays faster than  $e^{-\lambda^* x}$ ) will asymptotically approach the traveling front solution with the minimum wave speed  $c^* = c(\lambda^*)$ . Note that  $c^* \sim \sigma$  and  $\lambda^* \sim \sigma^{-1}$ .

One of the most important properties of nonlinear diffusion equations supporting pulled fronts is that the long-time convergence of steep initial conditions towards the pulled front solution is universal in leading and subleading order with respect to an asymptotic expansion in  $1/\sqrt{t}$  [19]. This result generalizes to higher order PDEs, difference-differential equations and equations with a memory kernel. For a formal proof of this universal behavior using matched asymptotics, see Ebert and van

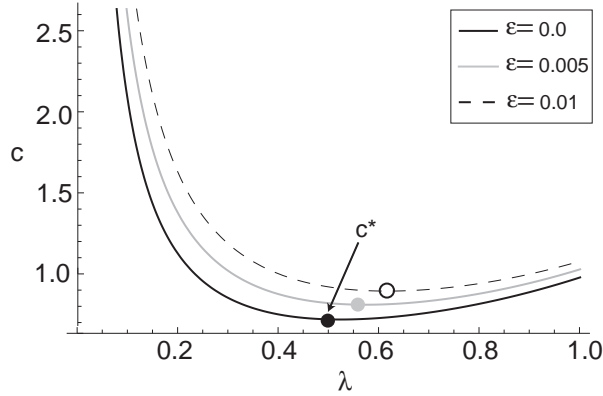


FIG. 4.1. Velocity dispersion curve (black) for a Gaussian weight distribution with  $\sigma = 1.0$  and  $W_0 = 1.2$ . Minimum wave speed is  $c^* = 0.71$ . Also shown are shifted dispersion curves in the presence of multiplicative noise for various noise amplitudes  $\varepsilon$  and  $C(0) = 10$  (see §4.2).

Saarloos [19]. Unfortunately, this analysis cannot be applied straightforwardly to the neural field equation (4.1) with  $F$  given by equation (4.3), since the nonlinear rate function has a discontinuous first derivative. Nevertheless, it is still possible to give a heuristic argument for the asymptotic convergence to the pulled front, which can also be found in [19]. Linearizing equation (4.1) about  $a = 0$  gives

$$\frac{\partial a(x,t)}{\partial t} = -a(x,t) + \int_{-\infty}^{\infty} w(x-x')a(x',t)dx'. \quad (4.11)$$

An arbitrary initial condition  $a(x,0)$  will evolve under equation (4.11) as

$$a(x,t) = \int_{-\infty}^{\infty} G(x-y,t)a(y,0)dy, \quad (4.12)$$

where  $G(x,t)$  is the Green's function

$$G(x,t) = \int_{-\infty}^{\infty} e^{ikx - i\omega(k)t} \frac{dk}{2\pi} \quad (4.13)$$

and

$$\omega(k) = i\widehat{W}(ik). \quad (4.14)$$

Given a sufficiently steep initial condition, for which the Fourier transform of  $a(x,0)$  is analytic, the asymptotic behavior of  $a(x,t)$  can be obtained from the large-time asymptotics of  $G(x,t)$  based on steepest descents. The latter will depend on the frame of reference. In a uniformly moving frame  $\xi = x - ct$ , we have

$$G(\xi,t) = \int_{-\infty}^{\infty} e^{ik\xi - i[\omega(k) - ck]t} \frac{dk}{2\pi}. \quad (4.15)$$

In the limit  $t \rightarrow \infty$  and fixed  $\xi$ , we can deform the  $k$ -contour to go through the saddle point  $k^*$  in the complex  $k$  plane where  $\omega(k) - ck$  varies least, that is,

$$\frac{d[\omega(k) - ck]}{dk} = 0 \implies c = \left. \frac{d\omega(k)}{dk} \right|_{k^*}. \quad (4.16)$$

The integral will then be dominated by the contribution in a neighborhood of the saddle. (If there are several saddle points then the dominant one will be the saddle with the maximal growth rate). Expanding the integral expression for the Green's function about the saddle to second order leads to the Gaussian approximation

$$G(\xi, t) = e^{ik^*\xi - i[\omega(k^*) - ck^*]t} \psi(\xi, t) \quad (4.17)$$

with

$$\psi(\xi, t) \approx \int_{-\infty}^{\infty} e^{i(k-k^*)\xi - \mathcal{D}(k-k^*)^2} = \frac{e^{-\xi^2/(4\mathcal{D}t)}}{\sqrt{4\pi\mathcal{D}t}} \quad (4.18)$$

and

$$\mathcal{D} = \frac{i}{2} \left. \frac{d^2\omega(k)}{dk^2} \right|_{k^*}. \quad (4.19)$$

It is important not to confuse the diffusion coefficient  $\mathcal{D}$  associated with the asymptotics of a deterministic pulled front with the diffusion coefficient  $D$  associated with the effects of noise on the stochastic wandering of a front.

For general speeds  $c$ , the growth or decay rate of the Fourier mode at the saddle, which is given by  $\text{Im}[\omega(k^*) - ck^*]$ , will be non-zero. The linear spreading velocity is then defined as the one for which there is zero growth rate [19], so that

$$c^* = \frac{\text{Im} \omega(k^*)}{\text{Im} k^*}, \quad (4.20)$$

which supplements equation (4.16). Let  $k_i = \text{Im} k^*$ ,  $k_r = \text{Re} k^*$ ,  $\omega_i = \text{Im} \omega(k^*)$  and  $\omega_r = \text{Re} \omega(k^*)$ . Equating real and imaginary parts in equation (4.16) and using the Cauchy–Riemann relations shows that  $c^* = d\omega_i/dk_i$  and  $0 = d\omega_i/dk_r$ . As with all the examples considered in [19], we find that  $k_r = 0$  and  $\omega_r = 0$  for a Gaussian weight distribution. Equations (4.14), (4.16) and (4.20) then imply that  $c^* = c(\lambda^*)$  as before, with  $\lambda^* = k_i$ . Moreover,  $\mathcal{D}$  is positive and real with

$$\mathcal{D} = \frac{\lambda^*}{2} \left. \frac{d^2c(\lambda)}{d\lambda^2} \right|_{\lambda^*}. \quad (4.21)$$

Positivity of  $\mathcal{D}$  follows from the fact that  $\lambda^*$  is a minimum of  $c(\lambda)$ . We conclude from the asymptotic analysis of the linear problem (4.11) that, given a sufficiently localized initial condition, we have the long-time solution  $a(x, t) \sim e^{-\lambda^*\xi} \psi(\xi, t)$  where  $\xi = x - c^*t$  and the so-called leading edge variable  $\psi(\xi, t)$  satisfies the diffusion equation

$$\frac{\partial\psi}{\partial t} = \mathcal{D} \frac{\partial^2\psi}{\partial \xi^2} + \text{h.o.t.} \quad (4.22)$$

As previously pointed out by Ebert and van Saarloos [19], although the spreading of the leading edge under linearization gives the right qualitative behavior, it fails to match correctly the traveling front solution of the full nonlinear system. In particular, the asymptotic front profile takes the form  $\mathcal{A}(\xi) \sim \xi e^{-\lambda^*\xi}$  for  $\xi \gg 1$ . The factor of  $\xi$  reflects the fact that at the saddle point the two branches of the velocity dispersion curve  $c(\lambda)$  meet, indicating a degeneracy. If one considers the asymptotic behaviour of the solution of the full nonlinear neural field equation, we find that in the asymptotic

regime  $\xi \gg 1, t \gg 1$ , we have a linear equation whose Green's function can be analyzed as before using steepest descents. In particular, we obtain a leading edge variable  $\psi(\xi, t)$  that satisfies a diffusion equation. Hence, in order to match the  $\xi e^{-\lambda^* \xi}$  asymptotics of the front solution we follow [19] and take the so-called dipole solution of the diffusion equation

$$\psi(x, t) = -\partial_\xi \frac{e^{-\xi^2/(4\mathcal{D}t)}}{\sqrt{4\pi\mathcal{D}t}} = \xi \frac{e^{-\xi^2/(4\mathcal{D}t)}}{\sqrt{2\pi}(2\mathcal{D}t)^{3/2}}. \quad (4.23)$$

Putting all of this together, we expect the leading edge to relax asymptotically as

$$a \sim \xi e^{-\lambda^* \xi} e^{-\xi^2/(4\mathcal{D}t)} t^{-3/2} \quad (4.24)$$

with  $\xi = x - v^*t$ . Finally, writing

$$e^{-\lambda^* \xi} t^{-3/2} = e^{-\lambda^* [x - v^*t - X(t)]}, \quad X(t) = -\frac{3}{2\lambda^*} \ln t, \quad (4.25)$$

suggests that to leading order the velocity relaxes to the pulled velocity  $v^*$  according to (see also [19])

$$v(t) = v^* + \dot{X}(t) = v^* - \frac{3}{2\lambda^* t} + h.o.t. \quad (4.26)$$

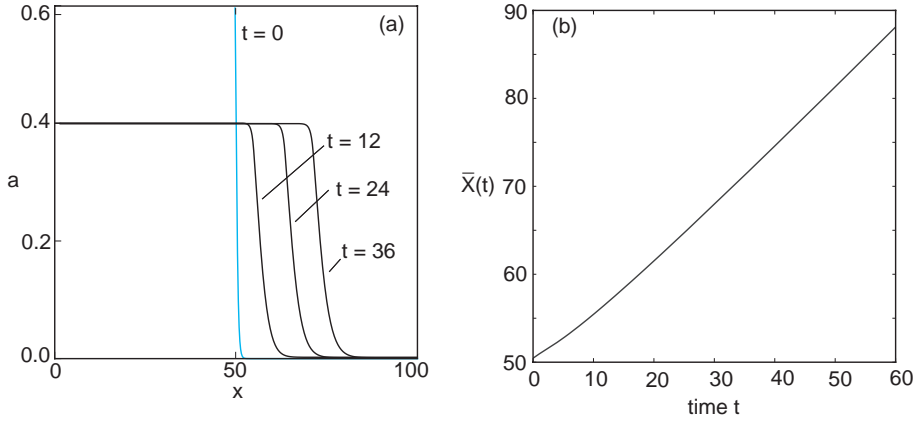


FIG. 4.2. Propagation of a pulled front solution of the neural field equation (4.1) with piecewise linear firing rate function (4.3) and a Gaussian weight distribution (4.6). Here  $W_0 = 1.2, \sigma = 1.0$  and  $\kappa = 0.4$ . (a) Snapshots of the front profile evolving from an initial condition consisting of a steep sigmoid function of unit amplitude (light blue curve). (b) Plot of mean displacement  $\bar{X}(t)$  as a function of time  $t$ .

In the above analysis we have made two major assumptions. First, that the piecewise-linear neural field equation (4.1) and (4.3) supports the propagation of a pulled front rather than a pushed front; in the latter case velocity selection would depend on the full nonlinear system. Second, given the existence of a pulled front, the asymptotic convergence to the front exhibits universal features also found for the nonlinear diffusion equation even though the nonlinearity is piecewise smooth. These assumptions appear to be confirmed by numerical solutions of equation (4.1). In Fig.

4.2(a) we show snapshots of a traveling front evolving from an initial condition consisting of a steep sigmoid. The corresponding mean displacement is a linear function of time (see Fig. 4.2(b)) with a slope  $c \approx 0.68$  consistent with the minimal wave speed  $c^* = 0.71$  of Fig. 4.1. Such a wave speed was also found for other values of  $\kappa$ . The universal nature of the asymptotic convergence of the wave speed to its final value independent of the height of the wave (level set) is illustrated in Fig. 4.3

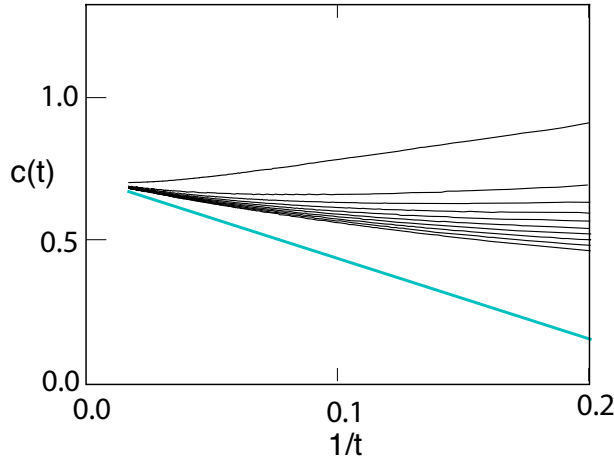


FIG. 4.3. Plot of wave speed  $v(t)$  as a function of inverse time  $1/t$  for various front amplitudes (level sets). Straight blue line is analytical expression for speed given by equation (4.26). All parameters as in Fig. 4.2.

#### 4.2. Subdiffusive fluctuations in the presence of multiplicative noise.

In the case of the F-KPP equation with multiplicative noise, it has previously been shown that the stochastic wandering of a pulled front about its mean position is subdiffusive with  $\text{var}\Delta(t) \sim t^{1/2}$ , in contrast to the diffusive wandering of a front propagating into a metastable state for which  $\text{var}\Delta(t) \sim t$  [43]. Such scaling is a consequence of the asymptotic relaxation of the leading edge of the deterministic pulled front. Since pulled front solutions of the neural field equation (4.1) exhibit similar asymptotic dynamics, see equation (4.24), it suggests that there will also be subdiffusive wandering of these fronts in the presence of multiplicative noise. In order to illustrate this, consider the Langevin equation

$$dA(x, t) = \left[ -A(x, t) + F \left( \int_{-\infty}^{\infty} w(x-y)A(y, t)dy \right) \right] dt + \varepsilon^{1/2}g_0A(x, t)dW(x, t) \quad (4.27)$$

with  $W(x, t)$  a Wiener process satisfying equation (2.12). Note that the noise term has to vanish when  $A(x, t) = 0$ , since the firing rate  $A$  is restricted to be positive. Hence, the noise has to be multiplicative. Formally speaking, we can carry over the analysis of the Langevin equation (2.11). First, the multiplicative noise leads to a modification in the mean speed of the front. That is, writing

$$A(x, t) = A_0(\xi - \Delta(t)) + \varepsilon^{1/2}\Phi(\xi - \Delta(t), t) \quad (4.28)$$

with  $\xi = x - ct$ , we find that the mean profile  $A_0$  satisfies the deterministic equation

$$-c\frac{dA_0}{d\xi} + A_0(\xi)[1 - \varepsilon g_0^2 C(0)] = F \left( \int_{-\infty}^{\infty} w(\xi - \xi')A_0(\xi')d\xi' \right). \quad (4.29)$$

The mean velocity of the pulled front is now given by the minimum of the dispersion curve  $c = c_\varepsilon$  where

$$c_\varepsilon(\lambda) = \frac{1}{\lambda} \left[ \widehat{W}(\lambda) + \widehat{W}(-\lambda) - [1 - \varepsilon g_0^2 C(0)] \right]. \quad (4.30)$$

Fluctuations thus shift the dispersion curve to higher velocities as shown in Fig. 4.1. However, it is no longer possible to derive an expression for the diffusion coefficient  $D(\varepsilon)$  along the lines of equation (2.27), since both numerator and denominator would diverge for a pulled front. This reflects the asymptotic behavior of the leading edge of the front. It is also a consequence of the fact that there is no characteristic time scale for the convergence of the front velocity to its asymptotic value, which means that it is not possible to separate the fluctuations into a slow wandering of front position and fast fluctuations of the front shape [19, 37].

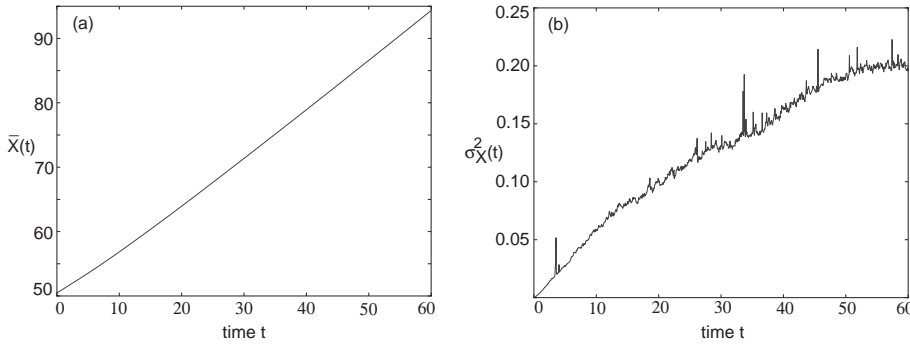


FIG. 4.4. Plot of (a) mean  $\bar{X}(t)$  and (b) variance  $\sigma_X^2(t)$  of the position of a stochastic pulled front as a function of time. Noise amplitude  $\varepsilon = 0.005$  and  $\kappa = 0.8$ . Other parameter values as in Fig. 4.2.

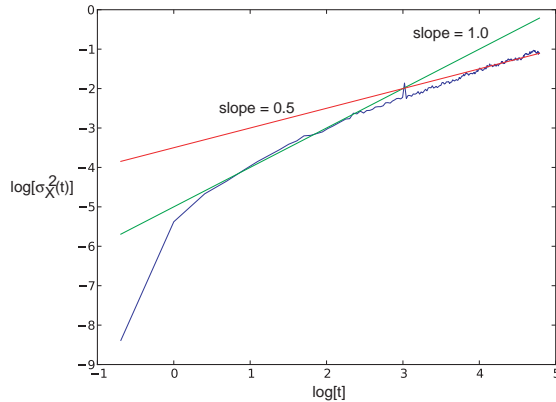


FIG. 4.5. Log-log plot of variance  $\sigma_X^2(t)$  as a function of time  $t$ . Same parameter values as Fig. 4.4.

Nevertheless, numerical simulations of equation (4.27) with  $F$  given by the piecewise linear firing rate (4.3) are consistent with subdiffusive wandering of the front. In

Fig. 4.4 we plot the mean  $\overline{X}(t)$  and variance  $\sigma_X^2(t)$  of the position of a pulled front solution of equation (4.27), which are obtained by averaging over level sets along identical lines to §2.3. It can be seen that  $\overline{X}(t)$  varies linearly with  $t$  with a slope equal to a speed  $c \approx 0.8$ , which is consistent with the shifted minimal wave speed, see Fig. 4.1 for  $\varepsilon = 0.005$ . Moreover, the variance appears to exhibit subdiffusive behavior over longer time scales. This is further illustrated by plotting a log-log plot of  $\sigma_X^2(t)$  against time  $t$ , see Fig. 4.5. It can be seen that at intermediate time-scales the slope of the curve is approximately equal to one, consistent with normal diffusion, but at later times the slope decreases, indicating subdiffusive behavior.

**4.3. Master equation for stochastic neural fields.** One of the interesting features of the neural field equation (4.1) is that it forms the starting point for a master equation formulation of stochastic neurodynamics [13, 14, 8, 9]. The latter treats a neural field as a continuum of interacting local populations. The state of each population is represented by the number of currently active neurons, and the state transitions of the associated discrete Markov process are chosen such that deterministic neural field equations of the form (4.1) are recovered in the thermodynamic limit  $N \rightarrow \infty$ , where  $N$  is the number of neurons in each local population. In order to develop the basic formalism, it is simpler to start off with a spatially discrete network and take the continuum limit at the end.

Thus, suppose that there exist  $M$  homogeneous local neuronal populations labeled  $i = 1, \dots, M$ , each of size  $N$ . Assume that all neurons of a given population are equivalent in the sense that the effective pairwise synaptic interaction between a neuron of population  $i$  and a neuron of population  $j$  only depends on  $i$  and  $j$ . Suppose that there are  $N_k(t)$  active neurons in the  $k$ th population. The state or configuration of the network is now specified by the vector  $\mathbf{N}(t) = (N_1(t), N_2(t), \dots, N_M(t))$ , where each  $N_i(t)$  is treated as a stochastic variable that evolves according to a one-step jump Markov process. Let  $P(\mathbf{n}, t) = \text{Prob}[\mathbf{N}(t) = \mathbf{n}]$  denote the probability that the network of interacting populations has configuration  $\mathbf{n} = (n_1, n_2, \dots, n_M)$  at time  $t, t > 0$ , given some initial distribution  $P(\mathbf{n}, 0)$ . The probability distribution is then taken to evolve according to a master equation of the form [13, 14, 8]

$$\frac{dP(\mathbf{n}, t)}{dt} = \sum_{k=1}^M \sum_{r=\pm 1} [T_{k,r}(\mathbf{n} - r\mathbf{e}_k)P(\mathbf{n} - r\mathbf{e}_k, t) - T_{k,r}(\mathbf{n})P(\mathbf{n}, t)]. \quad (4.31)$$

Here  $\mathbf{e}_k$  denotes the unit vector whose  $k$ th component is equal to unity. The corresponding transition rates are given by

$$T_{k,-1}(\mathbf{n}) = n_k, \quad T_{k,+1}(\mathbf{n}) = NF \left( \sum_l w_{kl} n_l / N \right), \quad (4.32)$$

where  $w_{kl}$  is the effective synaptic weight distribution from the  $l$ th to the  $k$ th population. Equation (4.31) is supplemented by the boundary conditions  $P(\mathbf{n}, t) \equiv 0$  if  $n_i = -1$  for some  $i$ . The master equation preserves the normalization condition  $\sum_{n_1 \geq 0} \sum_{n_M \geq 0} P(\mathbf{n}, t) = 1$  for all  $t \geq 0$ . Now introduce the rescaled variables  $a_k = n_k / N$  and corresponding transition rates

$$\Omega_{k,-1}(\mathbf{a}) = a_k, \quad \Omega_{k,+1}(\mathbf{a}) = F \left( \sum_l w_{kl} a_l \right). \quad (4.33)$$

Carrying out a Kramers–Moyal expansion to second order then leads to the multi-variate Fokker–Planck equation

$$\frac{\partial P(\mathbf{a}, t)}{\partial t} = - \sum_{k=1}^M \frac{\partial}{\partial a_k} [V_k(\mathbf{a})P(\mathbf{a}, t)] + \frac{\epsilon}{2} \sum_{k=1}^M \frac{\partial^2}{\partial a_k^2} [B_k(\mathbf{a})P(\mathbf{a}, t)] \quad (4.34)$$

with  $\epsilon = N^{-1}$ ,

$$V_k(\mathbf{a}) = \Omega_{k,1}(\mathbf{a}) - \Omega_{k,-1}(\mathbf{a}), \quad B_k(\mathbf{a}) = \Omega_{k,1}(\mathbf{a}) + \Omega_{k,-1}(\mathbf{a}). \quad (4.35)$$

The solution to the Fokker–Planck equation (4.34) determines the probability density function for a corresponding stochastic process  $\mathbf{A}(t) = (A_1(t), \dots, A_M(t))$ , which evolves according to a neural Langevin equation of the form

$$dA_k = V_k(\mathbf{A})dt + \epsilon^{1/2}b_k(\mathbf{A})dW_k(t). \quad (4.36)$$

with  $b_k(\mathbf{x})^2 = B_k(\mathbf{x})/2$ . Here  $W_k(t)$  denotes an independent Wiener process such that

$$\langle dW_k(t) \rangle = 0, \quad \langle dW_k(t)dW_l(s) \rangle = 2\delta_{k,l}\delta(t-s)dtds. \quad (4.37)$$

We can now take the continuum limit of the above Langevin equation along the lines outlined in [8]. Suppose that there is a uniform density  $\rho$  of neuronal populations distributed along the  $x$ -axis. We partition the  $x$ -axis into discrete intervals of length  $\Delta x$  within which there are  $\rho\Delta x$  populations. Let us denote the set of populations in the interval  $[m\Delta x, (m+1)\Delta x)$  by  $\mathcal{N}(m\Delta x)$ . As a further approximation, suppose that the weights  $w_{kl}$  are slowly varying on the length-scale  $\Delta x$  so that we can write  $w_{kl} = w(m\Delta x, n\Delta x)$  for all  $k \in \mathcal{N}(m\Delta x)$  and  $l \in \mathcal{N}(n\Delta x)$ . It follows that

$$\sum_l w_{kl}A_l = \sum_n \omega(m\Delta x, n\Delta x) \sum_{l \in \mathcal{N}(n\Delta x)} A_l.$$

Define the local spatially averaged activity variable  $A(n\Delta x)$  according to

$$A(n\Delta x) = \langle A_l \rangle \equiv \frac{1}{\rho\Delta x} \sum_{l \in \mathcal{N}(n\Delta x)} A_l \quad (4.38)$$

where  $\rho\Delta x$  is the number of populations in each set  $\mathcal{N}(n\Delta x)$ . Performing a local population averaging of the Langevin equation (4.36) with respect to  $k \in \mathcal{N}(m\Delta x)$ , and making the mean field approximation  $\langle b_k(\mathbf{A})dW_k \rangle = b_k(\langle \mathbf{A} \rangle)\langle dW_k \rangle$  then gives<sup>1</sup>

$$dA(m\Delta x, t) = \left[ -A(m\Delta x, t) + F \left( \rho\Delta x \sum_n w(m\Delta x, n\Delta x)A(n\Delta x) \right) \right] dt + \epsilon^{1/2}g_m[\mathbf{A}]dW(m\Delta x, t), \quad (4.39)$$

<sup>1</sup>Note that equation (4.39) would be exact in the case of additive noise under the local homogeneity assumption for the synaptic weights. However, performing the local averaging with respect to  $k \in \mathcal{N}(m\Delta x)$  in the case of multiplicative noise is nontrivial. At the very least, some form of perturbation expansion in  $\epsilon$  would be needed in order to determine corrections to the mean field approximation. The issue of local population averaging has been addressed in some detail within the context of spatially discrete versions of equation (2.1) with additive noise, where the nonlinearity  $F$  appears inside the sum over weights [23].

where

$$g_m[A] = \sqrt{A(m\Delta x, t) + F\left(\rho\Delta x \sum_n w(m\Delta x, n\Delta x)A(n\Delta x)\right)} \quad (4.40)$$

and  $W(m\Delta x, t) = (\rho\Delta x)^{-1} \sum_{k \in \mathcal{N}(m\Delta x)} W_k(t)$ . Thus,  $\langle dW(m\Delta x, t) \rangle = 0$  and

$$\begin{aligned} \langle dW(m\Delta x, t)dW(n\Delta x, t) \rangle &= \frac{1}{(\rho\Delta x)^2} \sum_{k \in \mathcal{N}(m\Delta x)} \sum_{l \in \mathcal{N}(n\Delta x)} \langle dW_k(t)dW_l(s) \rangle \\ &= \frac{1}{\rho\Delta x} \delta_{m,n} \delta(t-s) dt ds. \end{aligned} \quad (4.41)$$

Finally, setting  $x = m\Delta x, y = n\Delta x$  and taking the continuum limit  $\Delta x \rightarrow 0$  with  $\rho^{1/2}W(m\Delta x, t) \rightarrow W(x, t)$ ,  $\rho w(m\Delta x, n\Delta x) \rightarrow w(x, y)$  and  $A(m\Delta x, t) \rightarrow A(x, t)$ , we obtain a neural field Langevin equation of the form (4.27), except that now the multiplicative noise term is nonlocal:

$$g_0 A(x, t) \rightarrow \rho^{-1/2} \sqrt{A(x, t) + F\left(\int_{-\infty}^{\infty} w(x, y)A(y, t)dy\right)}. \quad (4.42)$$

We conclude that under the Langevin and local mean field approximations, the master equation reduces to a stochastic neural field equation with nonlocal multiplicative noise, which in the thermodynamic limit  $N \rightarrow \infty$  or  $\varepsilon \rightarrow 0$  reduces to the deterministic neural field equation (4.1). Note, however, that in contrast to the previous examples, the multiplicative noise is Ito rather than Stratonovich.

Previously, Buice and Cowan [13] have used path integral methods and renormalization group theory to establish that a master equation formulation of neural field theory that evolves according to equation (4.1) in the deterministic limit belongs to the universality class of directed percolation, and consequently exhibits power law behavior suggestive of many measurements of spontaneous cortical activity *in vitro* and *in vivo* [3, 41]. One crucial assumption of their theory is that the neural field supports a zero absorbing state, which holds provided that the rate function satisfies  $F(0) = 0$ . In light of our current study, we see that another feature of this master equation is that the underlying deterministic mean field equation (4.1) supports a propagating pulled front. Such a front is particularly sensitive to the effects of fluctuations in the leading edge of the front. This has important implications for front solutions of the underlying master equation, where discreteness effects (in space and in the number of active neurons) play a crucial role within the leading edge of the front. That is, there is a fundamental quantum of activity within a local population consisting of a single active neuron, that is,  $A = 1/N$ . In other words, there is an effective lower cut-off within the leading edge of the front. In the case of nonlinear reaction diffusion equations, such discreteness effects have been shown to have a significant effect on the asymptotic velocity of a pulled front [12, 37]. It would be interesting to explore how such results carry over to neural field master equations with nonlocal interactions.

**5. Discussion.** In this paper we have explored the effects of multiplicative noise on front propagation in a one-dimensional scalar neural field with excitatory nonlocal connections. We have shown that the effects of noise on the wandering of the mean front position depends on properties of the underlying deterministic front. In the case of a freely propagating front linking a stable and metastable state, we find diffusive

wandering with the mean square displacement growing linearly with time  $t$ . On the other hand, if the front is locked to a moving stimulus, then the wandering is described by an Ornstein-Uhlenbeck process and the mean square displacement saturates in the long time limit. Finally, in the case of a pulled front linking a stable and unstable state, propagation is very sensitive to noise in the leading edge of the front and wandering becomes subdiffusive. The sensitivity to noise could also have important implications for traveling front solutions of the master equation formulation of stochastic neural fields.

One possible application of our work would be to explore the role of noise in the propagation of binocular rivalry waves. Previously we shown how some form of local adaptation such as synaptic depression is needed in order to break the symmetry between the left and right eye neural fields, thus allowing a front to propagate [10]. Such a front represents a perceptual switching wave, in which activity invades the suppressed eye network and retreats from the previously dominant eye network. In order to extend our analysis of stochastic front propagation, it will be necessary to consider a vector-valued neural field consisting of two pairs of activity and adaptation variables, one for each eye. One interesting issue concerns whether or not there are differences between the effects of noise in the adaptation variables compared with noise in the activity variables. Finally, in most studies of disinhibited cortical slices, waves take the form of pulses rather than fronts so that is is also important to develop techniques for analyzing pulse propagation in stochastic neural fields.

**Appendix.** Here we present a derivation of equation (2.13), see also [44]. Consider the Langevin equation

$$dU(x, t) = \left[ -U(x, t) + \int_{-\infty}^{\infty} w(x-y)F(U(y, t))dy \right] dt + \varepsilon^{1/2}g(U(x, t))dW(x, t) \quad (\text{A.1})$$

with (in the limit  $\lambda \rightarrow 0$ )

$$\langle dW(x, t) \rangle = 0, \quad \langle dW(x, t)dW(x', t) \rangle = \delta(x-x')dt. \quad (\text{A.2})$$

It is convenient to restrict  $x$  to a bounded domain,  $-L/2 \leq x \leq L/2$ , and to impose periodic boundary conditions. We can then introduce the discrete Fourier series

$$U(x, t) = \frac{1}{L} \sum_n e^{ik_n x} U_n(t), \quad W(x, t) = \frac{1}{L} \sum_n e^{ik_n x} W_n(t) \quad (\text{A.3})$$

with  $k_n = 2\pi n/L$  and  $W_n(t)$  an independent Wiener process such that

$$\langle dW_n(t) \rangle = 0, \quad \langle dW_n(t)dW_m(t) \rangle = 2L\delta_{m+n,0}dt. \quad (\text{A.4})$$

Fourier transforming equation (A.1) gives

$$dU_n(t) = [-U_n(t) + w_n F_n(t)]dt + \frac{\varepsilon^{1/2}}{L} \sum_m g_{n-m}(t)dW_m(t), \quad (\text{A.5})$$

where  $w_n$  is the  $n$ th Fourier coefficient of the weight distribution  $w(x)$ , and  $F_n, g_n$  are the Fourier coefficients of the time dependent functions  $F \circ U(t)$  and  $g \circ U(t)$  respectively. The associated Stratonovich Fokker-Planck equation takes the form [26]

$$\frac{\partial P}{\partial t} = - \sum_l \frac{\partial}{\partial u_l} [(-u_l + w_l F_l)P] + \frac{\varepsilon}{L} \sum_{l,m,q} \frac{\partial}{\partial u_l} g_{l-q} \frac{\partial}{\partial u_m} g_{m+q} P. \quad (\text{A.6})$$

Multiplying both sides of this equation by  $u_n$  and integrating with respect to  $u_m$ , integer  $m$ , leads to the following evolution equation for the mean:

$$\frac{d\langle U_n \rangle}{dt} = -\langle U_n \rangle + w_n \langle F_n \rangle + \frac{\varepsilon}{L} \sum_{m,q} \left\langle \frac{\partial g_{n-q}}{\partial U_m} g_{m+q} \right\rangle. \quad (\text{A.7})$$

Finally, taking the inverse transform of equation (A.7) gives

$$\begin{aligned} \frac{d\langle U(x,t) \rangle}{dt} &= -\langle U(x,t) \rangle + \int w(x-y) \langle F(U(y,t)) \rangle dy \\ &\quad + \frac{\varepsilon}{\Delta x} \langle g(U(x,t)) g'(U(x,t)) \rangle, \end{aligned} \quad (\text{A.8})$$

where we have used the result  $\partial g_n / \partial U_m = [g'(U)]_{n-m}$ . Note that it is necessary to introduce a cut-off in the frequencies, which is equivalent to introducing a fundamental lattice spacing of  $\Delta x$ . Alternatively, the multiplicative noise can be taken to have a small but finite correlation length in space so that  $C(0) = 1/\Delta x$ . Comparison of equation (A.7) with the mean of equation (A.1) yields the desired result.

#### REFERENCES

- [1] S Amari. Dynamics of pattern formation in lateral inhibition type neural fields. *Biol. Cybern.*, 27:77–87, 1977.
- [2] J Armero, J Casademunt, L Ramirez-Piscina, and J M Sancho. Ballistic and diffusive corrections to front propagation in the presence of multiplicative noise. *Phys. Rev. E*, 58:5494–5500, 1998.
- [3] J M Beggs and D Plenz. Neuronal avalanches are diverse and precise activity patterns that are stable for many hours in cortical slice cultures. *J. Neurosci.*, 24: 5216, 2004.
- [4] H Berestycki, G Nadin, B Perthame and L Ryzhik. The non-local Fisher-KPP equation: traveling waves and steady states. *Nonlinearity* 22, 2813, 2009.
- [5] R Blake and N Logothetis. Visual competition. *Nat. Rev. Neurosci.*, 3:1–11, 2002.
- [6] C A Brackley and M S Turner. Random fluctuations of the firing rate function in a continuum neural field model. *Phys. Rev. E*, 75:041913, 2007.
- [7] P C Bressloff (2001). Traveling fronts and wave propagation failure in an inhomogeneous neural network. *Physica D*, 155:83–100.
- [8] P C Bressloff. Stochastic neural field theory and the system-size expansion. *SIAM J. Appl. Math.*, 70:1488–1521, 2009.
- [9] P C Bressloff. Metastable states and quasicycles in a stochastic wilson-cowan model of neuronal population dynamics. *Phys. Rev. E*, 85:051903, 2010.
- [10] P C Bressloff and M Webber. Neural field model of binocular rivalry waves. *J. Comput. Neurosci.*, in press, 2011.
- [11] P C Bressloff. Spatiotemporal dynamics of continuum neural fields. Invited topical review, submitted to *J. Phys. A*, 2011.
- [12] E Brunet and B Derrida. Shift in the velocity of a front due to a cutoff. *Phys. Rev. E* 56:2597–2604.
- [13] M Buice and J D Cowan. Field-theoretic approach to fluctuation effects in neural networks. *Phys. Rev. E*, 75:051919, 2007.
- [14] M Buice, J D Cowan, and C C Chow. Systematic fluctuation expansion for neural network activity equations. *Neural Comp.*, 22:377–426, 2010.
- [15] S Coombes and M R Owen. Evans functions for integral neural field equations with Heaviside firing rate function. *SIAM J. Appl. Dyn. Syst.*, 4:574–600, 2004.
- [16] S Coombes. Waves, bumps and patterns in neural field theories. *Biol. Cybern.*, 93:91–108, 2005.
- [17] S Coombes and C R Laing. Pulsating fronts in periodically modulated neural field models. *Phys. Rev. E*, 83:011912, 2011.
- [18] S Coombes, C R Laing, H Schmidt, N Svanstedt and J A Wyller. Waves in random neural media, *Disc. Cont. Dyn. Syst. A*. In press, 2011.
- [19] U Ebert and W van Saarloos. Front propagation into unstable states: universal algebraic convergence towards uniformly translating pulled fronts. *Physica D* 146: 1-99, 2000.

- [20] G B Ermentrout and J B McLeod. Existence and uniqueness of travelling waves for a neural network. *Proc. Roy. Soc. Edin. A*, 123:461–478, 1993.
- [21] G B Ermentrout. Neural networks as spatio-temporal pattern-forming systems. *Rep. Prog. Phys.*, 61:353–430, 1998.
- [22] G B Ermentrout, J. Z. Jalicis and J. E. Rubin, Stimulus-driven traveling solutions in continuum neuronal models with a general smooth firing rate functions. *SIAM J. Appl. Math.* 70, 3039-3054, 2010.
- [23] O Faugeras, J Touboul, and B Cessac. A constructive mean-field analysis of multi-population neural networks with random synaptic weights and stochastic inputs. *Frontiers in Comp. Neurosci.*, 3:1–28, 2009.
- [24] R A Fisher. The wave of advance of advantageous genes *Ann. Eugenics* 7: 355, 1937.
- [25] S E Folias and P C Bressloff. Stimulus-locked traveling pulses and breathers in an excitatory neural network. *SIAM J. Appl. Math.*, 65:2067–2092, 2005.
- [26] J Garcia-Ojalvo and J M Sancho. External fluctuations in a pattern-forming instability. *Phys. Rev. E*, 53:5680–5689, 1996.
- [27] C W Gardiner. *Handbook of stochastic methods, 4th edition*. Springer, Berlin, 2009.
- [28] S A Gourley. Travelling front solutions of a nonlocal Fisher equation. *J. Math. Biol.* 41, 272-284, 2000.
- [29] X Huang, W C Troy, Q Yang, H Ma, C R Laing, S J Schiff, and J Wu. Spiral waves in disinhibited mammalian neocortex. *J Neurosci*, 24:9897–9902, 2004.
- [30] A Hutt, A Longtin, and L Schimansky-Geier. Additive noise-induces turing transitions in spatial systems with application to neural fields and the swift-hohenberg equation. *Physica D*, 237:755–773, 2008.
- [31] M Kang, D J Heeger, and R Blake. Periodic perturbations producing phase-locked fluctuations in visual perception. *J. Vision*, 9(2):8:1–12, 2009.
- [32] A. Kolmogorov, I Petrovsky and N Piscunov. Study of the diffusion equation with growth of the quantity of matter and its application to a biology problem. *Bull. Univ. Moskou Ser. Int. Se. A* 1: 1, 1937.
- [33] S H Lee, R Blake, and D J Heeger. Traveling waves of activity in primary visual cortex during binocular rivalry. *Nat. Neurosci.*, 8:22–23, 2005.
- [34] A S Mikhailov, L Schimansky-Geier and W Ebeling. Stochastic motion of the propagating front in bistable media. *Phys. Lett. A* 96: 453
- [35] J D Murray. *Mathematical Biology I: An introduction* Springer, New York, 2003.
- [36] E A Novikov. Functionals and the random-force method in turbulence theory. *Sov. Phys. JETP*, 20:1290, 1965.
- [37] D Panja. Effects of fluctuations on propagating fronts. *Phys. Rep.*, 393, 87-174, 2004.
- [38] F. de Pasquale, J Gorecki and J Poielawski. On the stochastic correlations in a randomly perturbed chemical front. *J. Phys. A* 25: 433, 1992.
- [39] D Pinto and G B Ermentrout. Spatially structured activity in synaptically coupled neuronal networks: I. traveling fronts and pulses. *SIAM J. Appl. Math.*, 62:206–225, 2001.
- [40] D Pinto, S L Patrick, W C Huang, and B W Connors. Initiation, propagation, and termination of epileptiform activity in rodent neocortex in vitro involve distinct mechanisms. *J. Neurosci.*, 25:8131–8140, 2005.
- [41] D Plenz and T C Thiagarajan. The organizing principles of neuronal avalanches: cell assemblies in the cortex? *Trends Neurosci.*, 30: 101, 2007.
- [42] K A Richardson, S J Schiff, and B J Gluckman. Control of traveling waves in the mammalian cortex. *Phys. Rev. Lett.*, 94:028103, 2005.
- [43] A Rocco, U Ebert, W. van Saarloos. Subdiffusive fluctuations of “pulled” fronts with multiplicative noise. *Phys. Rev. E* 65: R13, 2000.
- [44] F Sagues, J M Sancho, and J Garcia-Ojalvo. Spatiotemporal order out of noise. *Rev. Mod. Phys.*, 79:829–882, 2007.
- [45] L Schimansky-Geier, A S Mikhailov and W Ebeling. Effects of fluctuations on plane front propagation in bistable nonequilibrium systems. *Ann. Phys.* 40:277, 1983.
- [46] W. van Saarloos. Front propagation into unstable states. *Phys. Rep.* 386, 29-222, 2003.
- [47] H R Wilson, R Blake, and S H Lee. Dynamics of traveling waves in visual perception. *Nature*, 412:907–910, 2001.
- [48] L Zhang On stability of traveling wave solutions in synaptically coupled neuronal networks, (2003). *Differential and Integral Equations*, 16 5:513–536



## RECENT REPORTS

- |       |   |  |
|-------|---|--|
| 40/11 | Higher-order numerical methods for stochastic simulation of chemical reaction systems   | Székelly<br>Burrage<br>Erban<br>Zygalakis              |
| 41/11 | On the modelling and simulation of a high pressure shift freezing process   | Smith<br>Peppin<br>Ángel M. Ramos                      |
| 42/11 | An efficient implementation of an implicit FEM scheme for fractional-in-space reaction-diffusion equations                            | Burrage<br>Hale<br>Kay                                 |
| 43/11 | Coupling fluid and solute dynamics within the ocular surface tear film: a modelling study of black Line osmolarity                    | Zubkov<br>Breward<br>Gaffney                           |
| 44/11 | A prototypical model for tensional wrinkling in thin sheets   | Davidovitch<br>Schroll<br>Vella<br>Adda-Bedia<br>Cerde |
| 45/11 | A fibrocontractive mechanochemical model of dermal wound closure incorporating realistic growth factor                                | Murphy<br>Hall<br>Maini<br>McCue<br>McElwain           |
| 46/11 | A two-compartment mechanochemical model of the roles of transforming growth factor $\beta$ and tissue tension in dermal wound healing | Murphy<br>Hall<br>Maini<br>McCue<br>McElwain           |
| 47/11 | Effects of demographic noise on the synchronization of a metapopulation in a fluctuating environment                                  | Lai<br>Newby<br>Bressloff                              |
| 48/11 | High order weak methods for stochastic differential equations based on modified equations   | Abdulle<br>Cohen<br>Vilmart<br>Zygalakis               |
| 49/11 | The kinetics of ice-lens growth in porous media   | Style<br>Peppin  |
| 50/11 | Wound healing angiogenesis: the clinical implications of a simple mathematical model  | Flegg<br>Byrne<br>Flegg<br>McElwain                    |
| 51/11 | Wound healing angiogenesis: the clinical implications of a simple mathematical model  | Du<br>Gunzburger<br>Lehoucq<br>Zhou                    |
| 52/11 | Image Inpainting based on coherence transport with Adapted distance functions   | März   |

|       |   |   |
|-------|---|---|
| 54/11 | A multiple scales approach to evaporation induced Marangoni convection    | Hennessey<br>Münch                                    |
| 55/11 | The dynamics of bistable liquid crystal wells                             | Luo<br>Majumdar<br>Erban                              |
| 56/11 | Real-Time Fluid Effects on Surfaces using the Closest Point Method        | Auer<br>Macdonald<br>Treib<br>Schneider<br>Westermann |
| 57/11 | Isolating intrinsic noise sources in a stochastic genetic switch          | Newby   |
| 58/11 | Riemann-Cartan Geometry of Nonlinear Dislocation Mechanics                | Yavari<br>Goriely                                     |
| 59/11 | Helices through 3 or 4 points?  | Goriely<br>Neukirch<br>Hausrath                       |
| 60/11 | Bayesian data assimilation in shape registration                          | Cotter<br>Cotter<br>Vialard                           |
| 61/11 | Asymptotic solution of a model for bilayer organic diodes and solar cells | Richardson<br>Please<br>Kirkpatrick                   |
| 62/11 | Neural field model of binocular rivalry waves                             | Bressloff<br>Webber                                   |

**Copies of these, and any other OCCAM reports can be obtained from:**

**Oxford Centre for Collaborative Applied Mathematics  
Mathematical Institute  
24 - 29 St Giles'  
Oxford  
OX1 3LB  
England**

**[www.maths.ox.ac.uk/occam](http://www.maths.ox.ac.uk/occam)**